SEDIMENTOLOGY the journal of the International Association of Sedimentologists

*Sedimentology* (2014) **61**, 333–361 doi: 10.1111/sed.12058

# Evolution and architecture of a West Mediterranean Upper Pleistocene to Holocene coastal apron-fan system

STEFANO ANDREUCCI*,†, LAURA PANZERI‡, I. PETER MARTINI§, FRANCESCO MASPERO‡, MARCO MARTINI‡,¶ and VINCENZO PASCUCCI*

**Dipartimento di Scienze della Natura e del Territorio, Università di Sassari, via Piandanna 4, 07100 Sassari, Italy (E-mail: sandreucci@unica.it)*

*†Presently at Dipartimento di Scienze Chimiche e Geologiche, Università di Cagliari, via Trentino 51, 09127 Cagliari, Italy*

*‡CUDaM (Centro universitario per le datazioni di Milano-Bicocca) and Dipartimento di Scienza dei Materiali, Università di Milano-Bicocca, Via R. Cozzi 53, 20126 Milano, Italy*

*§School of Environmental Sciences, University of Guelph, Guelph, Ontario, Canada*

*¶INFN, Sezione di Milano Bicocca, Piazza della Scienza 1, I-20126 Milano*

## ABSTRACT

The Quaternary deposits of tectonically stable areas are a powerful tool to investigate high-frequency climate variations (<10 ka) and to distinguish allogenic and autogenic factors controlling deposition. Therefore, an Upper Pleistocene–Holocene coastal apron-fan system in north–western Sardinia (Porto Palmas, Italy) was studied to investigate the relations between climate changes, sea-level fluctuations and sediment source-supply that controlled its development. The sedimentary sequence records the strong influence of local (wet/dry) and worldwide (sea-level) environmental variations in the sedimentation and preservation of the deposits. A multi-disciplinary approach allowed subdivision of the succession into four major, unconformity-bounded stratigraphic units: U1 U2, U3 and U4. Unit U1, tentatively dated to the warm and humid Marine Isotopic Stage (MIS) 5, consists of sandy, gravelly coastal/beach deposits developed during high sea-level in low-lying areas. Unit U2 consists of debris-flow dominated fan-deposits (*ca* 74 ka; MIS 4), preserved as partial fills of small valleys and coves. Unit U2 is mainly composed of reddish silty conglomerate to pebbly siltstones sourced from the Palaeozoic metamorphic inland hills (bedrock), superficially disintegrated during the preceding warm, vegetation-rich MIS 5. The cold and semi-arid climate strongly reduced vegetation cover along the valley flanks. Therefore, sediment gravity-flow processes, possibly activated by rainstorms, led to deposition of debris-flow dominated fans. Unit U3 consists of water-flow dominated alluvial-fan deposits (*ca* 47 to 23 ka; MIS 3), developed on a slightly inclined coastal plain. Unit U3 is composed of sandstone and sandy conglomerate fed from two main sediment sources: metamorphic inland bedrock and Quaternary bioclastic-rich shelf-derived sands. During this cold phase, sea-level dropped sufficiently to expose bioclastic sands accumulated on the shelf. Frequent climate fluctuations favoured inland aeolian transport of sand during dry phases, followed by reworking of the aeolian bodies by flash floods during wet phases. Bedrock-derived fragments mixed with water-reworked, wind-blown sands led to the development of water-flow dominated fans. The Dansgaard–Oeschger events possibly associated with sand landward deflation and main fan formations are Dansgaard–Oeschger 13 (*ca* 47 ka), Dansgaard–Oeschger 8 (*ca* 39 ka) and Dansgaard–Oeschger 2 (*ca* 23 ka). No record of sedimentation during MIS 2 was observed. Finally, bioclastic-rich aeolianites (Unit U4, *ca* 10 to 5 ka;

 

MIS 1), preserved on a coastal slope, were developed during the Holocene transgression (*ca* 10 to 5 ka; MIS 1). The studied sequence shows strong similarities with those of other Mediterranean sites; it is, however, one of the few where the main MIS 4 and MIS 3 climatic fluctuations are registered in the sedimentary record.

**Keywords** Debris-flow dominated fan, dune-sourced alluvial fan, marine isotopic stages, Mediterranean Sea, OSL dating, water-flow dominated fan.

## INTRODUCTION

Numerous studies have been conducted on Quaternary colluvial and alluvial fans around the world, but only a few have investigated the presence, in a single coastal apron system, of adjacent debris-flow-dominated and stream-flow dominated alluvial fans (Chamyal *et al.*, 1997; Blikra & Nemec, 1998; Ritter *et al.*, 2000; Keefer *et al.*, 2003; Viseras *et al.*, 2003; Sohn *et al.*, 2007; Spencer & Robinson, 2008). In Arizona (USA), the presence of different bedrock sources allowed the contemporaneous formation of adjacent debris-flow and water-flow dominated alluvial fans, under the same climatic conditions (Blair, 1999a,b,c; Nichols & Thompson, 2005). In a coastal system on Crete, sediments from the same bedrock source built-up through time both debris-flow and water-flow dominated alluvial fans at the same locality under different climatic settings (Nemec & Postma, 1993). These authors pointed out that semi-arid conditions with occasional rainstorms led to the development of sediment gravity flow (debris flow) alluvial systems, whereas humid or monsoonal conditions activated powerful floods that built water-flood dominated alluvial fans. From other areas of the world, it has also been reported that alluvial fans were partially covered by or intercalated with wind-blown sandy sediments revealing a high-frequency fluctuation in the distribution of precipitation (Goodfriend *et al.*, 1996; Sweeney & Loope, 2001; Gardner *et al.*, 2006; Fornós *et al.*, 2009; Andreucci *et al.*, 2010; Coltorti *et al.*, 2010).

Much attention has recently been given to alluvial fans developed during the last glacial stage (Nott *et al.*, 2001, 2007). One of the major factors controlling alluvial fan development in a cold climate is the relative amount of humidity. In particular, Nott *et al.* (2001) have noted that relatively humid conditions during Marine Isotopic Stage (MIS) 3 led to the deposition of fanglomerates (water-flow dominated fans) mostly associated with major rainstorms. Debris-flow dominated fans, instead, developed during the colder and dryer MIS 2.

The objective of this article was to analyze the deposits of an Upper Pleistocene–Holocene fan-apron system cropping out along the rugged coasts of north–western Sardinia (West Mediterranean, Italy; Fig. 1A), to establish their age and to better understand the processes and palaeoenvironmental conditions that led to its formation in a tectonically stable area (Ferranti *et al.*, 2006). Specific questions that are addressed include the following: (i) how much global and local climate can influence the development of a fan-apron system; and (ii) what the roles of local topography and sediment supply are on system evolution?

### Geological and climate setting

Sardinia is composed mainly of metamorphic Palaeozoic rocks deformed during the Hercynian orogenesis (Carmignani *et al.*, 2001). These are locally overlain by Mesozoic rocks that have recorded repetitive marine transgressive and regressive episodes during their sedimentation. The Sardinia crustal block detached from the south-European plate during the lower Miocene and drifted to its present position at the eastern margin of the Balearic Basin (Fig. 1A; Doglioni *et al.*, 1999). During this migration, Sardinia was dissected by variously oriented transcurrent and normal faults that bound a series of half grabens filled with marine and continental deposits (Funedda *et al.*, 2003). During the early Pliocene, widespread volcanism and basin uplift occurred and the island suffered severe erosive phases (Carmignani *et al.*, 2001). From the late Pliocene a general low-thermal subsidence rate, 0·01 to 2 mm $a^{-1}$ (Ferranti *et al.*, 2006), led to the deposition of Pleistocene coastal succession mainly characterized by an alternating shallow marine and colluvial/aeolian deposits formed during major climatic and sea-level variations.

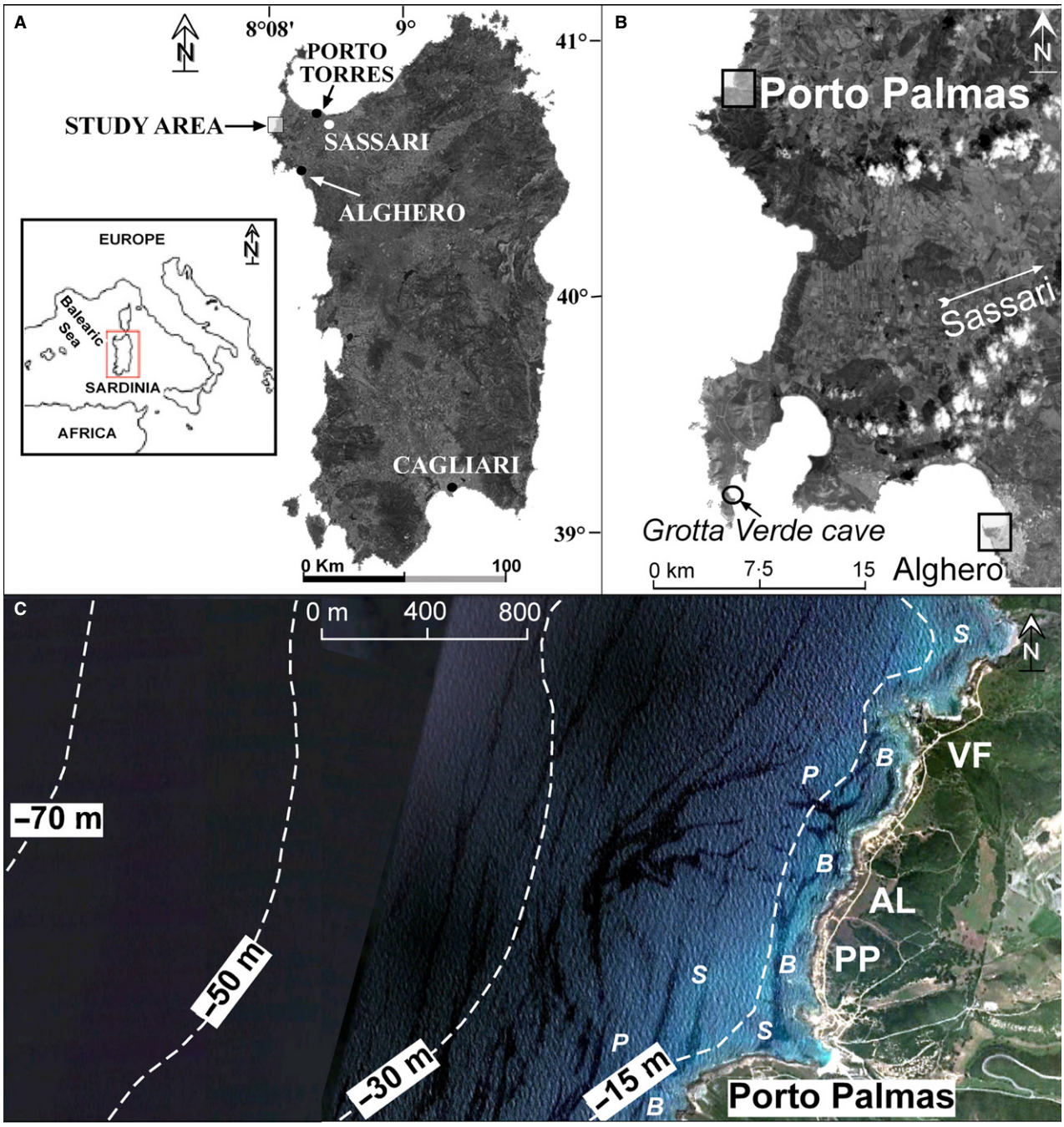


**Fig. 1.** Location map of the study area. (A) Satellite view of Sardinia and inset map of the west Mediterranean region. (B) Satellite view of north-western Sardinia and location of the Porto Palmas study area. (C) Aerial view and bathymetric map of the study area. Note the submerged bedrock 'B' up to −15 m below the present coastline followed by an extensive submerged bioclastic (temperate carbonate) sand plain 'S' with scattered *Posidonia oceanica* meadows 'P'. The sea grass meadow is the major sediment source for the pocket beaches of Porto Palmas. VF = narrow valleys/coves, AL = relatively flat coastal plain, PP = gently inclined hillslopes.

The coastal apron system studied here is located at the Porto Palmas site (Fig. 1B) and rests on Silurian, dark coloured, graphitic phyllites with quartz veins (Ginesu *et al.*, 2009). The Quaternary system includes several types of fan, beach and aeolian deposits that have two major sediment sources: (i) rocks composing the substrate of the hills; and (ii) Quaternary bioclastic sand generated on the shallow continental shelf.

The study area is dominated by a hilly landscape with coves bounded by bedrock cliffs and local sandy and gravelly pocket beaches rest on wave cut platforms (Fig. 1B). A 2 km long coastal hilly range up to 240 m high runs almost parallel to the coast (north–south; Figs 1C and 2A). The fan/coastal sedimentary system is subdivided, from north to south, into three main parts (Figs 1C and 2A): three narrow coves between high sea cliffs (Vf1, Vf2 and Vf3; Fig. 2A and B); gently sloping, narrow, coastal plains/terrace backed by the hill chain (Al1, Al2 and Al3; Fig. 2A and C); and slightly steeper hillslopes (PP1 and PP2; Fig. 2A). The approximate size of the various parts is as follows: the northernmost cove (Vf1) is 320 m wide at the exposed sedimentary section with an average bed dip of 15° towards the north–west; the second (Vf2) is 100 m wide and has a bed dip of 12° inclined towards the south–west; and the third cove (Vf3) is 60 m wide with an average bed dip of 10° towards the south–west. The alluvial fan Al1 is *ca* 170 m long (from the base of the hill to the present coastline) and 300 m wide with a surface dipping *ca* 6° towards the north–west, Al2 shows similar size but has a surface dipping at *ca* 5° to the west (Fig. 2C). The Al3 area is 170 m long and 230 m wide with a surface dipping *ca* 7° to the north–west. The third area (PP) is 500 m wide and characterized by a hill crest (PP1) and a valley flank (PP2).

A wide wave-cut platform, developed on the bedrock ('B' in Fig. 1C) at the coastline of the studied area is characterized by an irregular topography, related to intense deformation, with slight lows and highs extending into the shallow shelf up to a depth of 15 m below sea-level (Fig. 1C). Further out, the sea floor is covered by

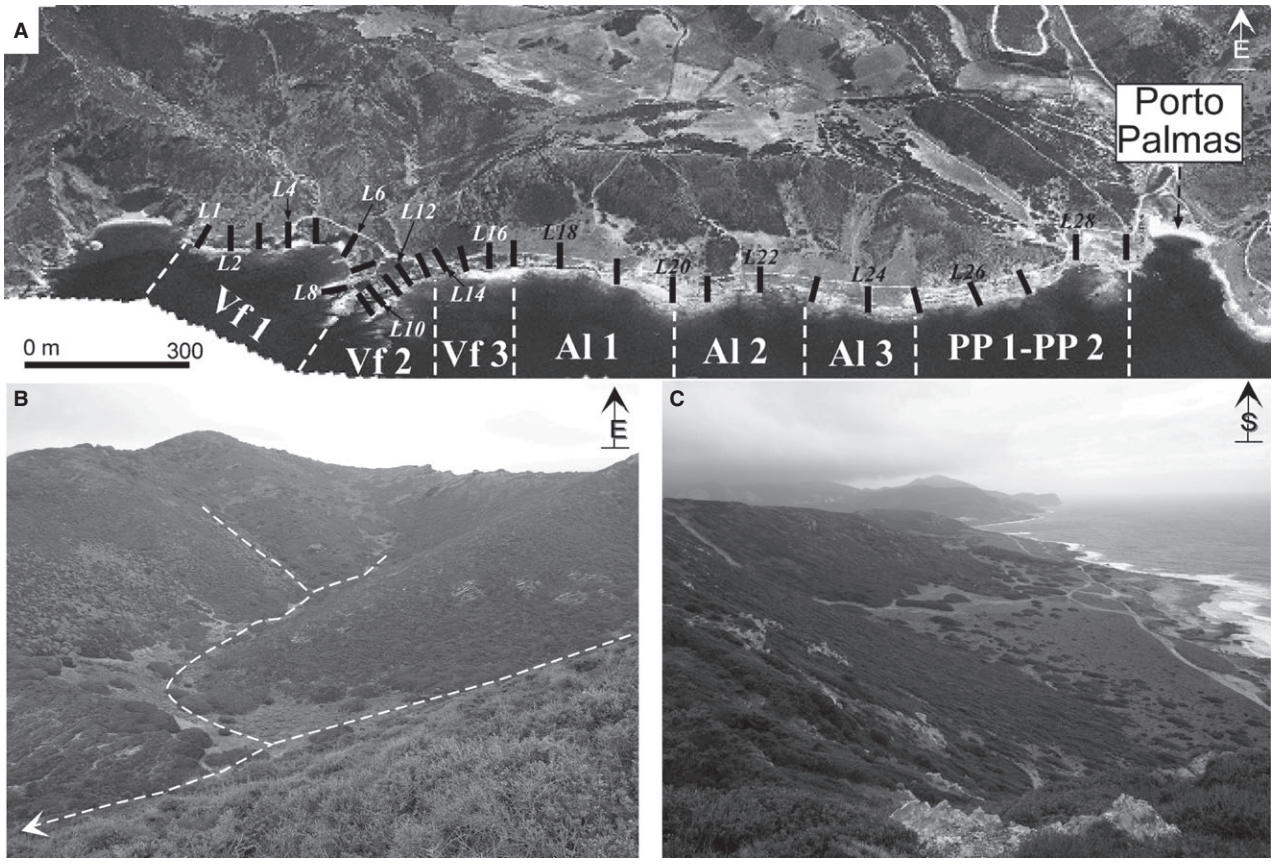


**Fig. 2.** (A) Three-dimensional view of the Porto Palmas area. The study site is subdivided into seven different depositional areas due to the bedrock topography: Vf = narrow valleys/coves between high sea cliffs (Vf1, Vf2 and Vf3); Al = small and relatively flat coastal plain backed by a hill chain (Al1, Al2 and Al3); PP = gently inclined hillslopes (PP1 and PP2); L1 = position of Log 1. (B) Detailed view of a narrow valley-head feeding the debris-flow dominated alluvial-fan system of Vf2. (C) Panoramic view of the water-flow dominated alluvial-fan system (Al1). Note the small and relatively steeply inclined inland hill chain (bedrock).

bioclastic sand (S) with scattered *Posidonia oceanica* meadows ('P'; Fig. 1C).

North–west Sardinia is characterized by a warm-temperate, marine climate with an average temperature ranging from 7°C in winter to *ca* 25°C in summer. It has a wet season (October to April), accounting for 80% of the yearly precipitation with frequent heavy rainstorm events, and a dry season (May to September; Delitala *et al.*, 2000). The dominant effective wind is from the north–west (*Mistral* wind) and is responsible for north–west/south–east longshore drift along the north–west coast of Sardinia (Donda *et al.*, 2008). The sea is microtidal with storm waves up to *ca* 7 m high [APAT (Agenzia per la Protezione dell'Ambiente per i servizi Tecnici), 2005]. The average sea temperature measured during 2008 at the Alghero bay (25 km to the south, Fig. 1A) was *ca* 20°C (APAT, 2010).

## METHODS

### Facies analysis and stratigraphy

Twenty-nine sections from the Upper Pleistocene–Holocene deposits cropping out along the Porto Palmas coast were measured and a facies analysis was performed (Fig. 2A). Recognized facies were named according to the main lithology, grain size, sedimentary structures and biogenic features (see Table 1 for more details on facies nomenclature). Facies interpretations are based on Bluck (1967) and Massari & Parea (1988) for shallow-marine deposits; Blair (1999a, b) for alluvial fan bodies and Livingstone & Warren (1996) for wind-blown strata.

Stratigraphic units were established and correlated according to sedimentary body lithologies and geometries, visible unconformities and key beds, such as palaeosols. Units were dated using optically stimulated luminescence (OSL) and radiometric ($^{14}$C) methods (Fig. 3; Tables 2 and 3).

### Optically stimulated luminescence method

The OSL method is suitable and has provided good results in dating terrigenous siliciclastic deposits of various aeolian, fluvial and coastal environments. The most reliable results tend to be obtained from aeolian deposits (e.g. Madsen & Murray, 2009; Thiel *et al.*, 2011), whereas less consistent results have been obtained for fluvial and alluvial deposits. Nevertheless, many OSL applications to fluvial and alluvial deposits have been successful (Bøe *et al.*, 2007; Buylaert *et al.*, 2007; Martins *et al.*, 2010; Pérez Alberti *et al.*, 2011; Andreucci *et al.*, 2012).

Eight samples from various units of the Porto Palmas deposits were treated under controlled red light conditions at the University of Sassari following the conventional procedure (Stokes, 1992; Mejdahl & Christiansen, 1994; Lang *et al.*, 1996; Mauz *et al.*, 2002) to separate pure quartz from K-feldspars. The OSL analysis was conducted at the CUDaM laboratory, University of Milano-Bicocca.

#### *Dosimetry*

For each sample, *ca* 200 g of sediment were collected to estimate the water content and to calculate the natural radioactivity (dose rate, $D_r$) (Table 2A). To estimate the dose rate, Th and U concentrations of each sample were measured with total alpha counting using ZnS scintillator discs (Aitken, 1985), assuming a concentration ratio Th/U equal to 3. Content of $^{40}$K was deduced from the total concentration of K measured with flame photometry.

Attenuation of the beta dose was taken into account (Bell, 1979). The cosmic ray contribution to the final dose rate was based on Prescott & Hutton (1994). The required correction on the $D_r$ values for cementation (lithified samples) were taken into account and calculated following Andreucci *et al.* (2012). A weighted average between the present-day and saturation values was selected as lifetime water content since the time of deposition for each sample (Table 2A).

The $^{40}$K internal radioactivity on K-feldspar grains contributing to the final dose rate was calculated assuming a K content of 12·0 ± 0·5% (Huntley & Baril, 1997). The concentrations of the principal radionuclides, average water content and dose rates are shown in Table 2A.

#### *Luminescence measurements and characteristics*

The OSL measurements were carried out using an automated Risø TL/OSL-DA-15 system (Risø, Roskilde, Denmark) equipped with a $^{90}$Sr/$^{90}$Y beta source. The quartz was stimulated by blue LEDs (470 ± 30 nm) and the luminescence detected through a U-340 filter. The K-feldspar was stimulated using an infrared (IR) diode array (830 ± 10 nm) and detection was through the standard blue filter pack (Schott BG-39 + Corning 7–59).

**Table 1.** Simplified description of the observed facies of the studied area. Facies are labelled using the following nomenclature: G = Conglomerate; S = Sandstone; W = reddish Siltstone; b = boulders to cobbles; c = cobbles to pebbles; d = pebbles to granules; e = medium to very coarse-grained sand; w = reddish silty-clay matrix; l = laminated; P = planar cross-bedded; t = trough cross-bedded; u = low-angle cross-bedded; m = massive; and r = root traces. Thus, facies labelled Sdu corresponds to sandstone (S) with pebbles to granules (d) and low-angle cross-beds (u); facies Wdm represents a massive (m) siltstone (W) with disseminated pebble to granule clasts (d). Facies interpretation based on Blair (1999a,b), Bluck (1967), Livingstone & Warren (1996) and Massari & Parea (1988).

| Facies | Characteristics | Transport process | Interpretation | Type image |
|---|---|---|---|---|
| **Gb** | Clast-supported conglomerate<br>- Angular clasts of phyllites and vein quartz<br>- Minor silty matrix (secondary)<br>- Steep inclined beds or lenses (>20°) | Sediment gravity flows | ***Bouldery rock fall deposit*** |  |
| **Gwb** | Matrix-supported conglomerate - Angular boulders to cobbles of phyllites and vein quartz<br>- Reddish silty matrix<br>Lenses: 1 m thick and 10 m long | Sediment gravity flows | ***Bouldery-cobbly debris flow dep.*** |  |
| **Gwc** | Matrix-supported conglomerate - Angular cobbles to pebbles of phyllites and vein quartz<br>-Reddish silty matrix<br>Lenses: 1 m thick and 20 m long | Sediment gravity flows | ***Cobbly-pebbly debris flow dep.*** | 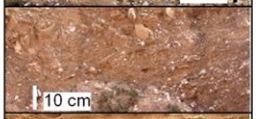 |
| **Scl** | Bioclastic & siliciclastic sandstone -angular pebbles of phyllites and vein quartz - Landward imbrication<br>-Poorly to fairly well sorted coarse-grained sand<br>- Terrestrial shells - Intense root bioturbation<br>- Main plane beds inclined 2°to 8° seaward | Un-confined water flows | ***Sandy-gravelly tabular sheetflood dep.*** | 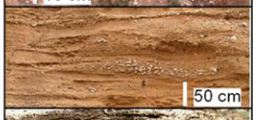 |
| **Scm** | Bioclastic and siliciclastic sandstone -pebbles of phyllites and vein quartz - Disseminated and lags<br>-Poorly to fairly well sorted coarse-grained sand<br>-Channel structures: 3 m deep/ 6 m wide | Confined water flows | ***Sandy-gravelly channels dep.*** |  |
| **Wdl** | Siltstone (red brown)-Mainly angular pebbles of phyllites and vein quartz<br>-Laminated with pebbly discontinuous lags | Sediment gravity flows | ***Silty-pebbly debris flow or soil creeping dep.*** |  |
| **Wdm** | Siltstone (dark reddish brown)-Angular pebbles of phyllites and vein quartz disseminated<br>-Root traces - Massive | Soil accumulation &/or colluviation | ***Silty-gravelly palaeosol dep.*** |  |
| **Selm** | Bioclastic sandstone - minor siliciclastic sand grains - Fairly well sorted medium to coarse-grained sand-Terrestrial shells - Intense root bioturbation - Plane beds up to 1 m thick | Wind flows | ***Aeolian sand sheet dep.*** | 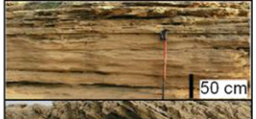 |
| **Sep(t)** | Bioclastic sandstone - minor siliciclastic sand grains - Fairly well sorted medium to coarse-grained sand-Terrestrial shells -Root bioturbation -Cross beds with 15-30° dips to SE | Wind flows | ***Aeolian sand dune dep.*** |  |
| **Gcl** | Clast-supported conglomerate - Rounded to sub-angular cobbles to pebbles of phyllites and vein quartz - Seaward imbrication<br>- Bioclastic & siliciclastic sand - Marine shells<br>- Lenticular thin layers | Marine waves &/or longshore currents | ***Gravelly submerged beachface dep.*** |  |
| **Gem** | Clast-supported conglomerate - Rounded phyllites & vein quartz- Megaboulders: 1 m D.<br>- Bioclastic & siliciclastic sand - Marine shells<br>- Massive with discontinuous lenses | Marine waves &/or longshore currents | ***Gravelly lag dep.*** |  |
| **Sdu** | Bioclastic & siliciclastic sandstone alternating with layer or lenses of well-rounded pebbles to granules clasts of vein quartz<br>- Marine shells - Thin low-angle inclined layers dipping seaward | Marine waves &/or longshore currents | ***Mixed sandy and gravelly submerged beachface dep.*** | 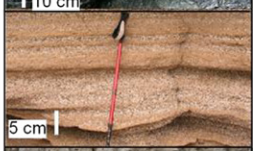 |
| **Seur** | Bioclastic & siliciclastic sandstone.<br>Rare layers of well rounded granules made of quartz - Marine shells - Low-angle cross-bedded dipping seaward-Root bioturabion at the top<br>- Massive at the top | Marine waves &/or longshore currents | ***Sandy beachface dep.*** |  |

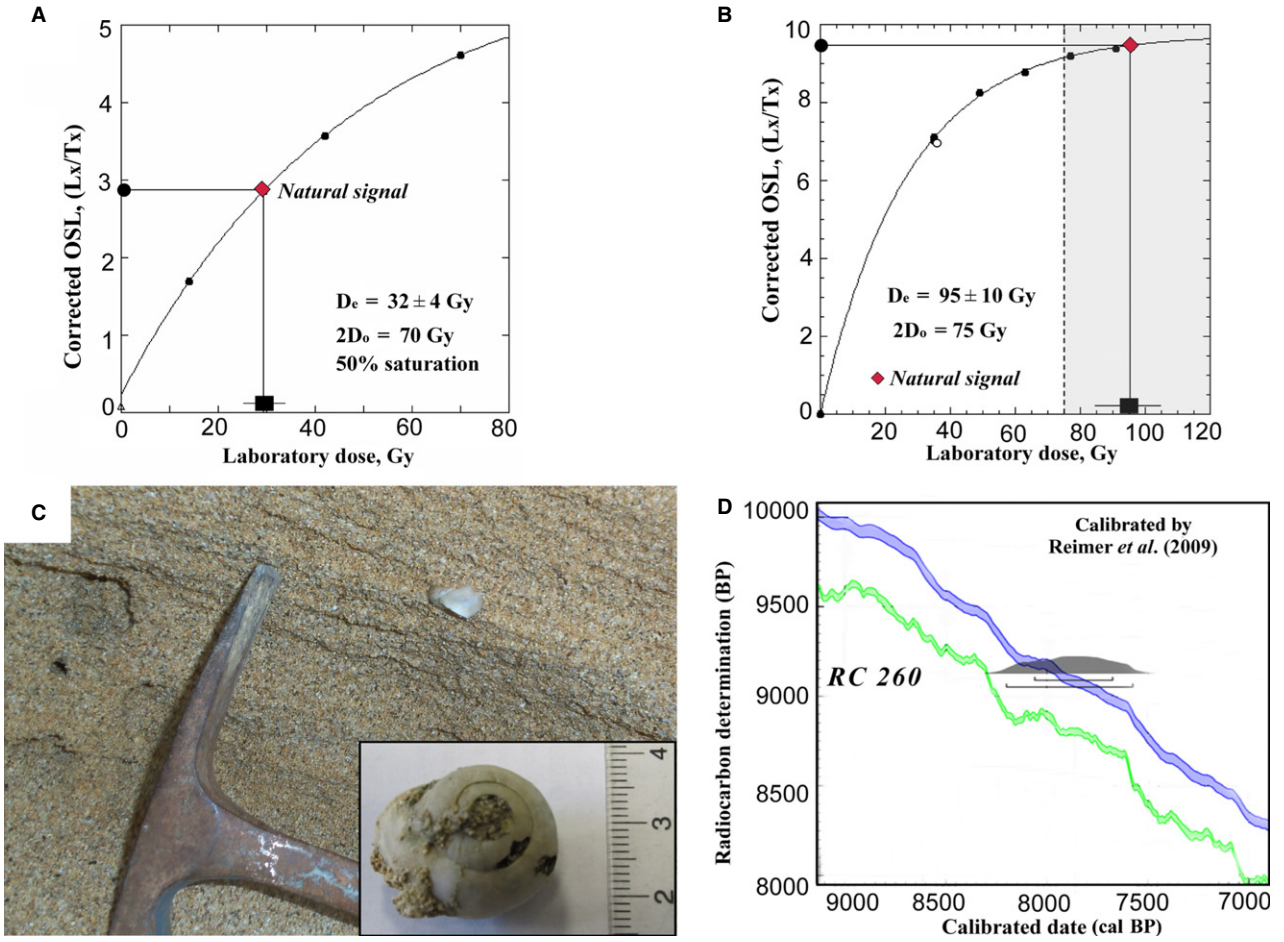


**Fig. 3.** (A) Quartz optically stimulated luminescence (OSL) Single Aliquot Regenerative(SAR)–growth curve for sample ARG7 based on three regenerative doses (small black circles). The diagram also shows: natural signal = red diamond and the Equivalent dose ($D_e$) = back square. Note that sample ARG7 is below the saturation limit ($D_e$ < 86% of 2Do). (B) Quartz OSL SAR-growth curve for sample ARG8 based on three regenerative doses (small black circles) and a recycling point (white circle). The diagram also shows: natural signal = red diamond and the Equivalent dose ($D_e$) = back square. Note that sample ARG8 is above the saturation limit ($D_e$ >86% of $2D_o$) indicated by the grey area. (C) Detailed view of the cross-stratified sandy deposits (aeolianites) from which a terrestrial shell (*Helix* spp.) was collected for radiometric analysis. Note that the shell is aligned to the strata. Inset is a detailed view of the sample RC260 used for radiocarbon dating. (D) Diagram showing the calibrated age based on the calibration curve of Reimer *et al.* (2009) expressed as 1$\sigma$ error from present.

Infrared stimulated luminescence was checked on quartz materials. This check proved negative (Smith *et al.*, 1990); therefore, a Single Aliquot Regenerative (SAR) protocol was used for equivalent dose ($D_e$) measurements (Murray & Wintle, 2000). The OSL measurements (100 sec) were made at 125°C, after pre-heating aliquots for 10 sec at 260°C. The pre-heat value was experimentally derived on the basis of the results of a dose recovery pre-heat plateau test. A cut-heat of 220°C was applied to each aliquot before the test dose measurement. The thermal transfer was systematically evaluated, calculating the recuperation point which never exceeded 5% of the natural. All aliquots had recycling values within the range of 1·0 ± 0·1 (Armitage *et al.*, 2000; Roberts & Wintle, 2001). All samples showed good OSL characteristics (such as high degree of inter-aliquot reproducibility) and a single aliquot distribution peak which is indicative of fully bleached, undisturbed sediments (Bateman *et al.*, 2007). Eight samples (ARG1 to ARG7 and ARG9) posses an equivalent dose ($D_e$) lower than 85% of the saturation point ($2 \times D_0$; Fig. 3A). Thus, the OSL age corresponds to a reliable indication of the sedimentary event (Wintle & Murray, 2006). Only ARG8 shows $D_e$ values beyond the satura-

**Table 2A.** Summary of quartz and K-feldspar optically stimulated luminescence dosimetry data including concentrations of major radioactive elements.

| Samples | Moisture (%) | Depth* (m) | U (ppm; ±5%) | Th (ppm; ±5%) | $^{40}$K (ppm; ±3%) | $D_r$ Qz (mGy a$^{-1}$) | $D_r$ K-feld (mGy a$^{-1}$) |
|---|---|---|---|---|---|---|---|
| Unit U4 | | | | | | | |
| ARG1 | 12·7 | 1·50 | 0·61 | 1·83 | 0·07 | 0·63 ± 0·04 | / |
| ARG2 | 13·3 | 2·00 | 0·91 | 2·73 | 0·11 | 0·76 ± 0·07 | / |
| ARG3 | 10·1 | 0·80 | 0·81 | 2·43 | 0·12 | 0·66 ± 0·03 | / |
| ARG4 | 13·1 | 1·50 | 0·66 | 1·98 | 0·11 | 0·58 ± 0·02 | / |
| ARG5 | 12·5 | 1·50 | 0·47 | 1·41 | 0·06 | 0·60 ± 0·05 | / |
| Unit U3 | | | | | | | |
| ARG6 | 13·4 | 1·00 | 1·02 | 3·06 | 0·31 | 0·91 ± 0·03 | / |
| ARG7 | 13·4 | 1·50 | 0·81 | 2·43 | 0·29 | 0·88 ± 0·13 | 1·09 ± 0·13 |
| ARG8 | 13·6 | 2·50 | 2·08 | 6·24 | 1·44 | 1·90 ± 0·12 | 2·18 ± 0·12 |
| Unit U2 | | | | | | | |
| ARG9 | 13·1 | 3·50 | 1·68 | 5·04 | 1·78 | 2·25 ± 0·13 | 2·65 ± 0·13 |

* Distance of the samples from the top of the outcrop. '/'denotes not measured with K-feldspar SAR post-IR IRSL (290) protocol because it is not reliable for young deposits (Thiel *et al.*, 2011).

**Table 2B.** Summary of quartz and K-feldspar dose equivalent ($D_e$) measurements and luminescence ages. The samples are arranged in the table so the first entry at the bottom represents the greatest age.

| Samples | $D_e$ Qz (Gy) | Qz age (ka) | $D_e$ K-feld (Gy) | K-feld age (ka) |
|---|---|---|---|---|
| Unit U4 | | | | |
| ARG1 | 3·1 ± 0·5 | 4·9 ± 0·8 | / | / |
| ARG2 | 5·1 ± 0·8 | 6·7 ± 1·1 | / | / |
| ARG3 | 5·2 ± 1·0 | 7·9 ± 1·6 | / | / |
| ARG4 | 4·7 ± 1·0 | 8.1 ± 1·7 | / | / |
| ARG5 | 6·0 ± 1·2 | 10 ± 2 | / | / |
| Unit U3 | | | | |
| ARG6 | 21 ± 4 | 23 ± 4 | / | / |
| ARG7 | 32 ± 4 | 36 ± 4 | 47 ± 3 | 43 ± 5 |
| ARG8 | Saturated* | – | 103 ± 4 | 47 ± 3 |
| Unit U2 | | | | |
| ARG9 | 168 ± 10 | 74 ± 9 | 198 ± 43 | 75 ± 4 |

The uncertainties are deviations on the mean (standard errors). * Equivalent dose ($D_e$) value is above the 86% of the saturation point (2 $D_o$). '/' denotes not measured with K-feldspar SAR post-IR IRSL(290) protocol because it is not reliable for young deposits (Thiel *et al.*, 2011).

tion point with the OSL data corresponding to a 'minimum' age (Table 2A). An example of growth curve for the saturated sample is shown in Fig. 3B.

K-feldspar SAR post-infrared stimulation (post-IR IRSL) at elevated temperature (290°C) protocol was applied to the samples with a quartz-OSL age older than 30 ka (ARG7 to ARG9; Thiel *et al.*, 2011). After preheat at 320°C for 60 sec, the samples were bleached with IR diodes at first at 50°C for 200 sec and then at 290°C for 200 sec. The same pre-heat conditions were used for regenerative and test doses. An IR illumination at 325°C for 100 sec was inserted at the end of each cycle. Generally, feldspar grains are affected by anomalous fading (Huntley & Lamothe, 2001); however, Buylaert *et al.* (2009) highlighted that applying high temperature at the SAR post-IR IRSL protocol should reduce the age correction for anomalous fading. The present authors tested samples for anomalous fading and did not find a relevant decay of the post-IR IRSL signal at 290°C two months after irradiation. The results obtained on quartz and K-feldspars are reported in Table 2B.

### Radiocarbon $^{14}C$ method

A terrestrial shell of *Helix* spp. aligned at the base of sandy strata was collected carving into the aeolianites at PP2 site (Figs 2A and 3C). Dating was performed at the CUDaM laboratory, University of Milano-Bicocca, by extracting the carbon isotopes from the sample via physical and chemical treatments. The sample was etched with a 1% HCl solution, and then $CO_2$ was extracted in a digestion reaction with phosphoric acid. The $CO_2$ collected was then reduced to carbon and measured at the LABEC facility of the INFN laboratory in Florence.

The $^{14}C/^{12}C$ and $^{13}C/^{12}C$ ratios were measured with accelerator mass spectrometry, from which the percentage of modern carbon (pMC), and the conventional age (tRC) of the samples have been evaluated (Table 3). The conventional dates were calibrated following the methodology of Bronk Ramsey (2009) and Reimer *et al.* (2009; OxCal v.4, INTCAL09 calibration curve), and converted into calibrated ages (Table 3 and Fig. 3D).

## RESULTS

### Lithofacies

The Porto Palmas apron system is characterized by a complex spatial (lateral and vertical) facies distribution building up variously stacked sedimentary bodies. Brief descriptions and interpretations of the established 13 major lithofacies are presented in Table 1. The facies show a vertical variation in marine deposits at the bottom overlain by continental strata. The lowest marine bodies are sandy and mixed sand and gravel beach deposits with a general shallowing and fining upward trend.

Continental strata are characterized by gravity-flow deposits, such as rock falls and debris flows, at the base of the succession in the northern part of the study area. These are overlain by water flow deposits produced by sheetfloods and channel fills, in the middle-upper part of the succession in the central part of the study area. Towards the southernmost part of the study area, wind blown deposits (aeolian sand sheets and sand dunes) cap the succession.

### Stratigraphy and depositional system

Correlations between the section-logs along the study area highlight the presence of four major unconformity-bounded units: U1, U2, U3 and U4 (Fig. 4). Each unit is described where best developed and its lateral variability along the different depositional areas (Vf, Al or PP) is discussed.

#### *Unit U1*

Unit U1 rests non-conformably over the metamorphic bedrock (surface A) and is composed of gravelly, sandy and mixed sand and gravel beach deposits. Unit U1 shows a great variability in facies and its preserved thickness is influenced by the local bedrock topography and coastal sediment transport (Fig. 4).

One of the most complete and thickest (4 m maximum) successions of Unit U1 is preserved at the seaward corner of the northern flank of the Vf1 cove (Figs 2A and 4 – Logs 1 to 4). There, the succession consists of a lower interval dominated by low-angle cross-laminated, well-sorted medium to coarse-grained sandstone alternated with thin, horizontal to slightly inclined beds of well-sorted, quartz pebble to granule sandy conglomerate (facies Sdu; Fig. 5A and B). The upper interval, instead, is characterized by sparsely fossiliferous, well-sorted, coarse-grained, cross-laminated sandstone (facies Seur), strongly bioturbated by root-traces at the top (Fig. 5A). The sandstone consists of 55 to 65% of marine bioclastic materials (fragments of red algae, molluscs, echinoids, benthic foraminifera and bryozoans) and 35 to 45% of siliciclastic grains (phyllite fragments, muscovite, quartz and K-rich feldspars; Fig. 5B). Marine fossils (mainly broken shells) include the following: *Cardita senegalensis, Glycymeris glycymeris*, *Ostrea* sp. and *Patella* sp. (Fig. 5C). These deposits represent a beach system ranging from the foreshore (facies Sdu and lower part of Seur) to the strongly bioturbated backshore (upper part of facies Seur).

**Table 3.** Summary of the radiometric ($^{14}C$) age. Calibrated dates are based on Reimer *et al.* (2009). See text and Fig. 3D for further details

| Code | pMC | tRC (BP years) | Calibrated date ($\pm 1\sigma$) | Calibrated date ($\pm 2\sigma$) |
|---|---|---|---|---|
| RC260 | 32·10 ± 0·46 | 9127 ± 116 | 8060 to 7675 BP | 8200 to 7575 BP |

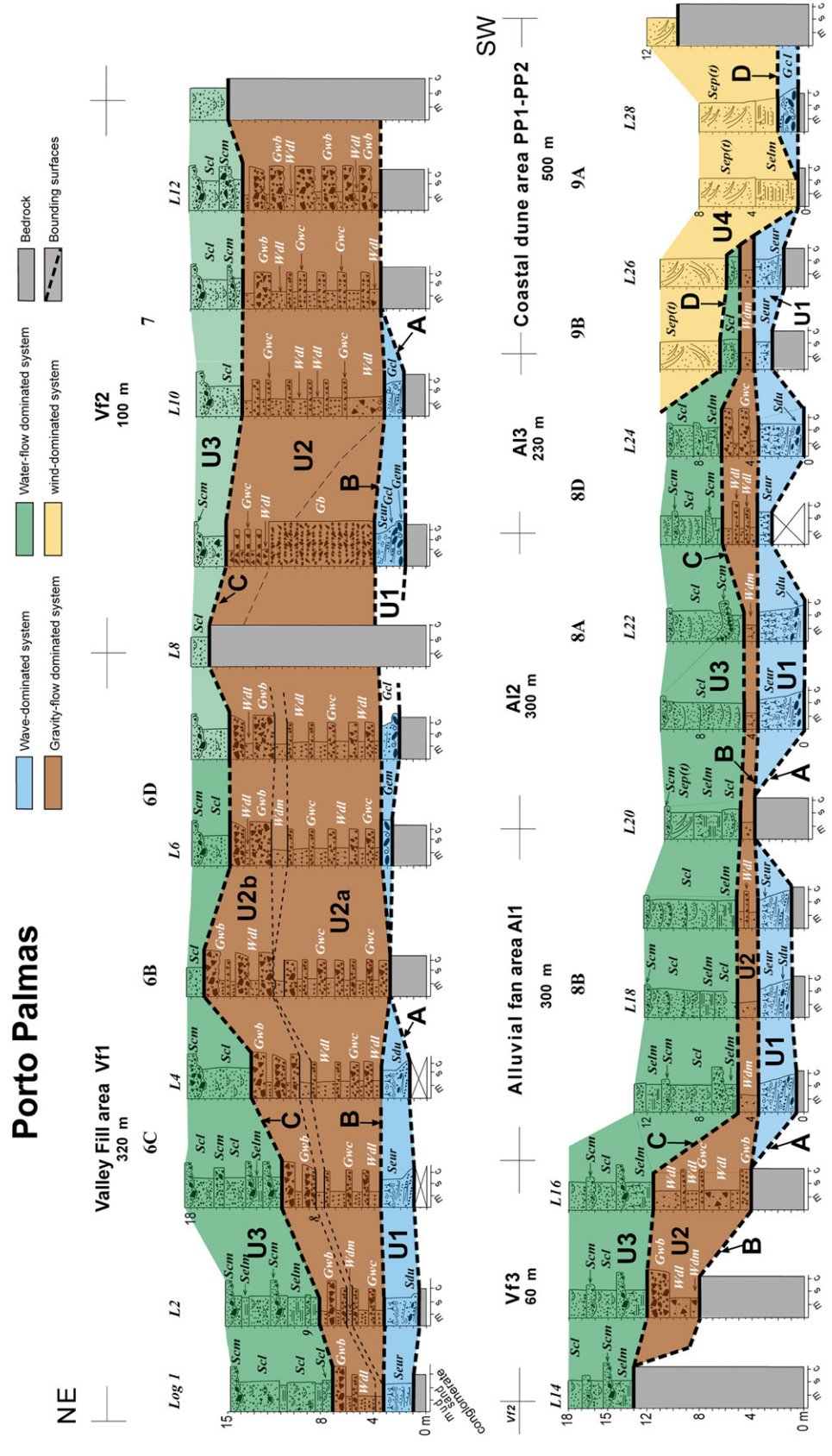


**Fig. 4.** Cross-section of stratigraphic sections measured in the Porto Palmas area (see Fig. 2 for the location). L1 = Log 1. U1 = unconformity bounded unit. Labels such as *Gwc* indicate facies described in the text and in Table 1. Bold numbers at the top of the logs correspond to figures showing details of the various areas.

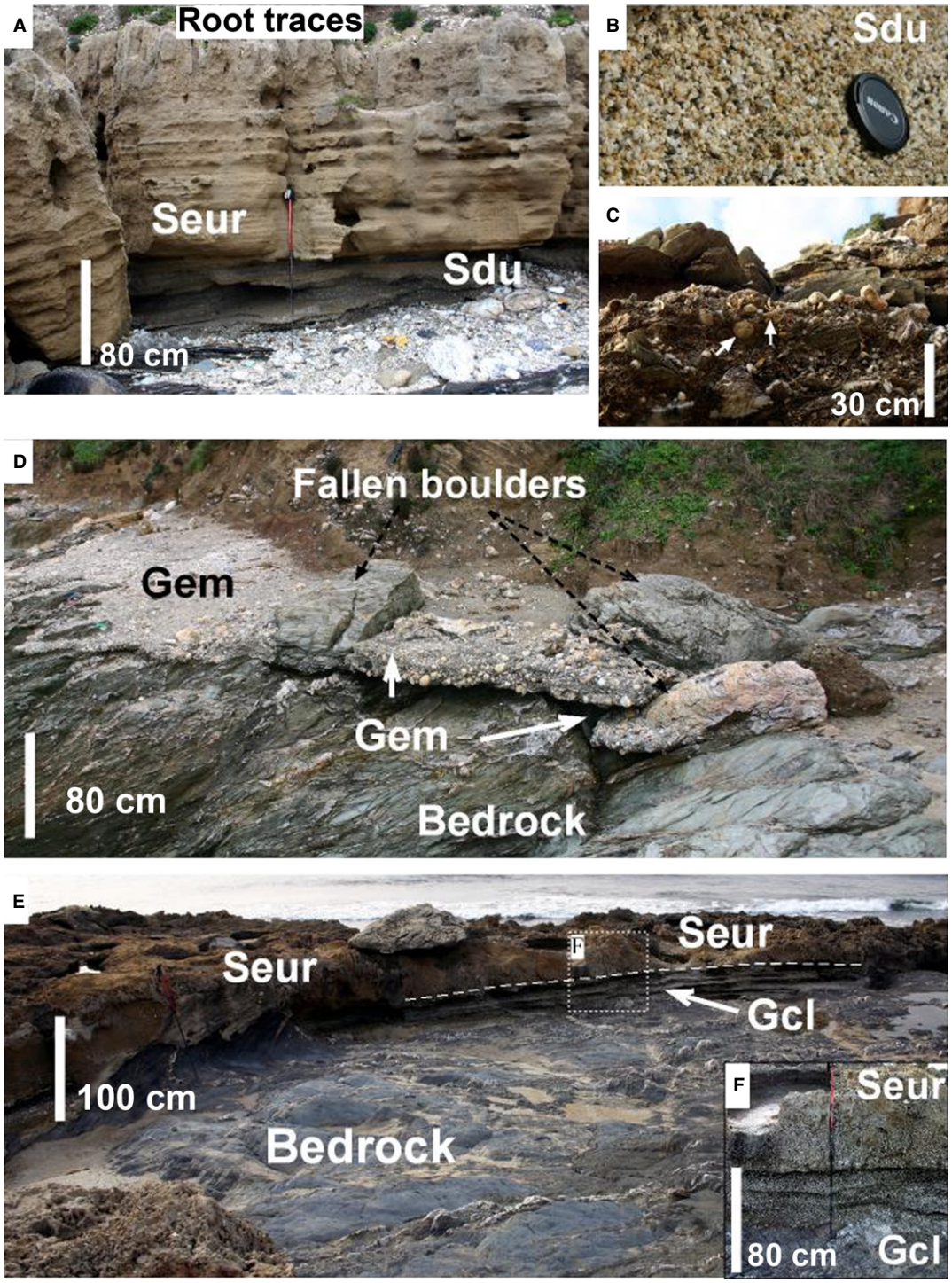


**Fig. 5.** Shallow-marine deposits of Unit U1. (A) Low-angle cross-stratified sandy-granules deposits 'Sdu' overlain by gently inclined layers of medium to coarse-grained sandy strata 'Seur'. Note that facies Seur, towards the top, is highly bioturbated by roots. (B) Detail of the sandy granules deposits 'Sdu'. Lens cap for scale, 7 cm in diameter. (C) Marine fossils (white arrows) in a coarse-grained pebbly beach deposit. (D) Facies 'Gem', composed of spherical to rounded pebbly-bouldery layers. Note that the boulders that have fallen from the adjacent cliffs. (E) Wave-cut bedrock platforms with residual lenses of sandy conglomerate and well-rounded, vein-quartz pebbles, alternating with laminated coarse-grained sandstone with a few disseminated fine pebbles (Facies 'Gcl'). (F) Beach deposit succession showing a shallowing upward trend from facies 'Gcl' to facies 'Seur'.

 

Along the inner landward side of coves, poorly sorted conglomerates form a thin (less than 1 m) basal lag over metamorphic basement rocks. The conglomerates are composed of sub-angular to well-rounded pebbles and cobbles of metamorphic and vein-quartz, respectively, surrounding large sub-angular metamorphic cobbles and boulders (facies Gem; Figs 4 and 5D – Log 6). It is most likely that these deposits were formed in the submerged zone of a gravel beach ('outerframe', *sensu* Bluck, 1967) where boulders fallen from the coastal backcliffs were partially rounded by wave actions. In other sections of cove Vf2 (Fig. 4 – Log 9), the basal coastal unit consists of poorly sorted, coarse gravel storm-deposits with sub-rounded vein-quartz pebbles and cobbles, sub-angular phyllite clasts and reworked marine shells, such as *C. senegalensis, G. glycymeris*, *Ostrea* sp. and *Patella* sp. (Fig. 5C).

Locally, on partially exposed wave-cut bedrock platforms of Al areas, thin (up to 3 m thick) residual lenses of sandy conglomerate occur, in which well-rounded, quartz pebbles alternate with laminated coarse-grained sandstone and few disseminated fine pebbles (Facies Gcl) (Fig. 5E and F). Some clasts show seaward imbrication. It is most likely that this deposit was formed in the lower part of the beachface zone (*sensu* Massari & Parea, 1988).

*Unit U2*

Unit U2 is delimited at the base by an unconformity (surface B, Fig. 4) that deeply cuts into Unit U1. This unit is almost exclusively composed of conglomeratic and silty deposits. Unit U2 is present everywhere except for the southern PP2 area (Fig. 4). It is interpreted as the product of debris-flow dominated alluvial fans, as demonstrated below.

Thick (15 m maximum) deposits of Unit U2, almost completely fill the narrow valleys and coves Vf1, Vf2 and Vf3. This unit is mainly composed of poorly sorted, massive silty conglomerate to pebbly siltstone with some siltstone layers of prevalent reddish brown colouration (5YR 5/4 – 5YR 4/6). The phyllite and vein-quartz clasts, ranging in size from pebble to local boulders, are sub-angular to angular in shape.

The deposits of the largest cove Vf1 vary both laterally and vertically (Fig. 6A to D). These deposits differ in two main depositional areas: in the central inland apex (core) area of the fan at the termination of a steep, narrow, feeding valley (Fig. 6B) and along the northern and southern flanks of the fan (Fig. 6C and D). Vertically U2 is separated into two parts (U2a and U2b) by an erosional surface (Fig. 6B) or by a rather continuous, fairly well-developed palaeosol (Fig. 6C and D; facies Wdm, Table 1).

The U2a deposits of the central core area are characterized by thick chaotic agglomerations of bouldery to cobble-pebbly debris-flow deposits (facies Gwb and Gwc) with some erosion-remnant layers of silt including sparse, small phyllite pebbles and granules (facies Wdl; Fig. 6B). The core deposits grade outward along the valley flanks into progressively finer-grained, thinner-bedded bodies (Fig. 6C). In the lateral/distal zones, the deposits of the U2a unit consist of thin beds of silty pebbly conglomerate to pebbly siltstone arranged in a fining upward trend along section-logs and outward from the core to the distal part of the succession (Fig. 6C). In the lateral and distal zones, U2a deposits are capped by a

**Fig. 6.** (A) Panoramic view of the sedimentary succession filling up the narrow valley/cove area Vf1 with inset location map. From the bottom up: marine deposits of Unit U1 (resting on bedrock) followed by debris-flow dominated alluvial fan system (Unit U2), capped by sandy sheetflood deposits of U3. The white arrow indicates the trend of the feeding valley. (B) The central (core) zone of the Vf1 system. Note that deposits of Unit U2 directly rest on the bedrock (unconformity 'B') and are capped by sandy sheetflood deposits of U3 (unconformity 'C'). In the core zone, U2 is subdivided into subunits U2a and U2b based on an erosive surface (black solid line), variations in granulometry and structures. Key for facies is in Table 1. (C) Panoramic view of the left flank (lateral/distal part) of valley/cove fill Vf1. From the bottom up: marine deposits of Unit U1 resting on bedrock are overlaid by a debris-flow dominated fan of U2 and capped by a water-flow dominated system (U3). In the lateral/distal zone, U2 is subdivided into subunits U2a and U2b based on the presence of a well-developed 0·5 m thick palaeosol 'Wdm', variations in granulometry and structures. (D) Panoramic view of the right flank (lateral/distal part) of valley/cove fill Vf1. From the bottom up: wave-dominated system (U1) resting on bedrock (unconformity 'A'). Debris-flow dominated fan of U2 bounded at the base by the unconformity 'B' and at the top by the unconformity 'C'. Note that U2a and the palaeosol 'Wdm' are deeply eroded by coarse-grained debris-flow deposits 'Gwb' of U2b.

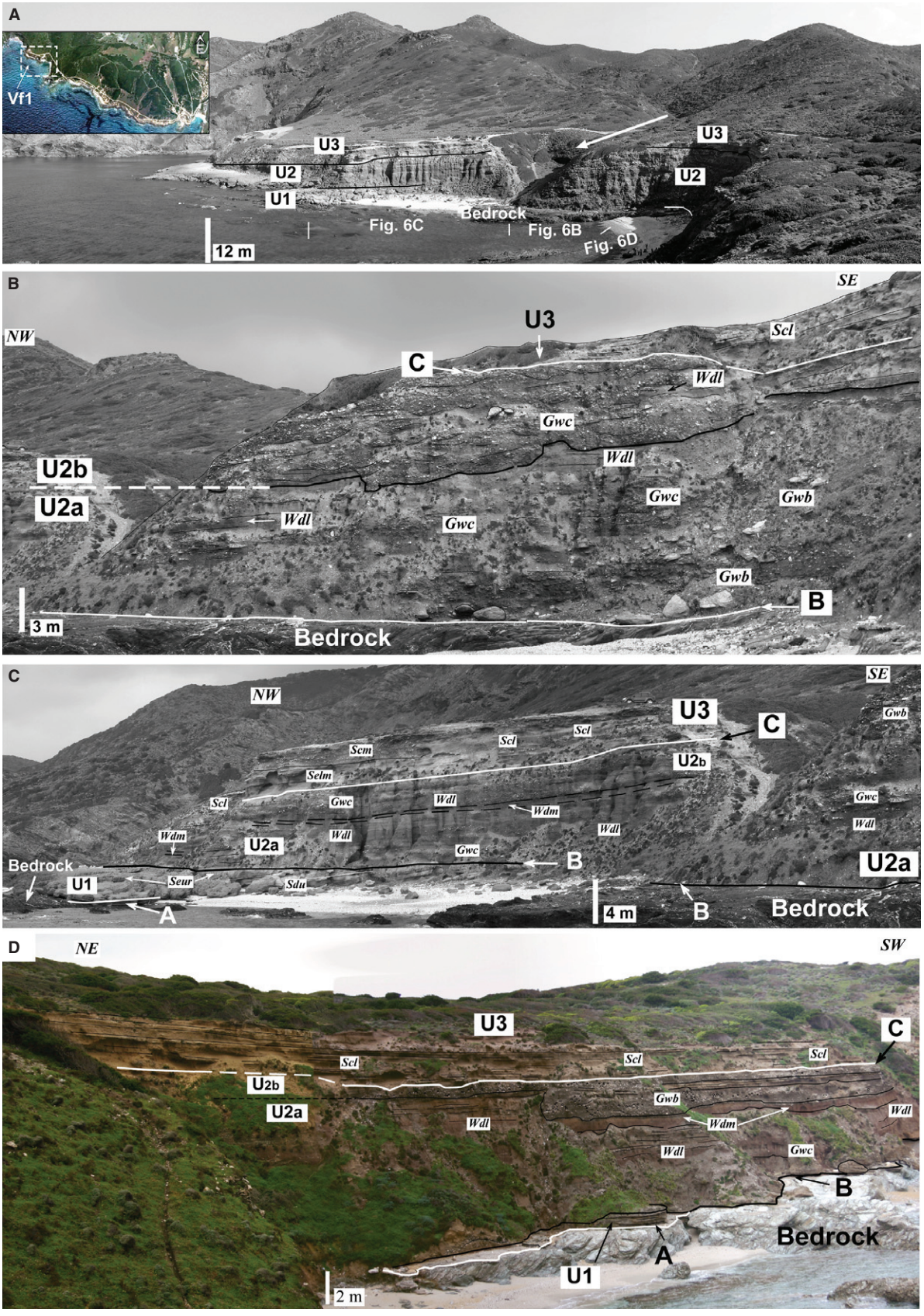
A
Vf1
U3
U2
U1
Fig. 6C
Bedrock
Fig. 6B
Fig. 6D
12 m
B
NW
SE
U3
C
Scl
Wdl
Gwc
U2b
U2a
Gwb
B
3 m
Bedrock
C
NW
SE
U3
C
Scm
Selm
U2b
Wdm
U2a
Bedrock
U1
Seur
Sdu
A
4 m
B
Bedrock
D
NE
SW
U3
C
U2b
U2a
Gwb
Wdm
B
A
U1
2 m
Bedrock

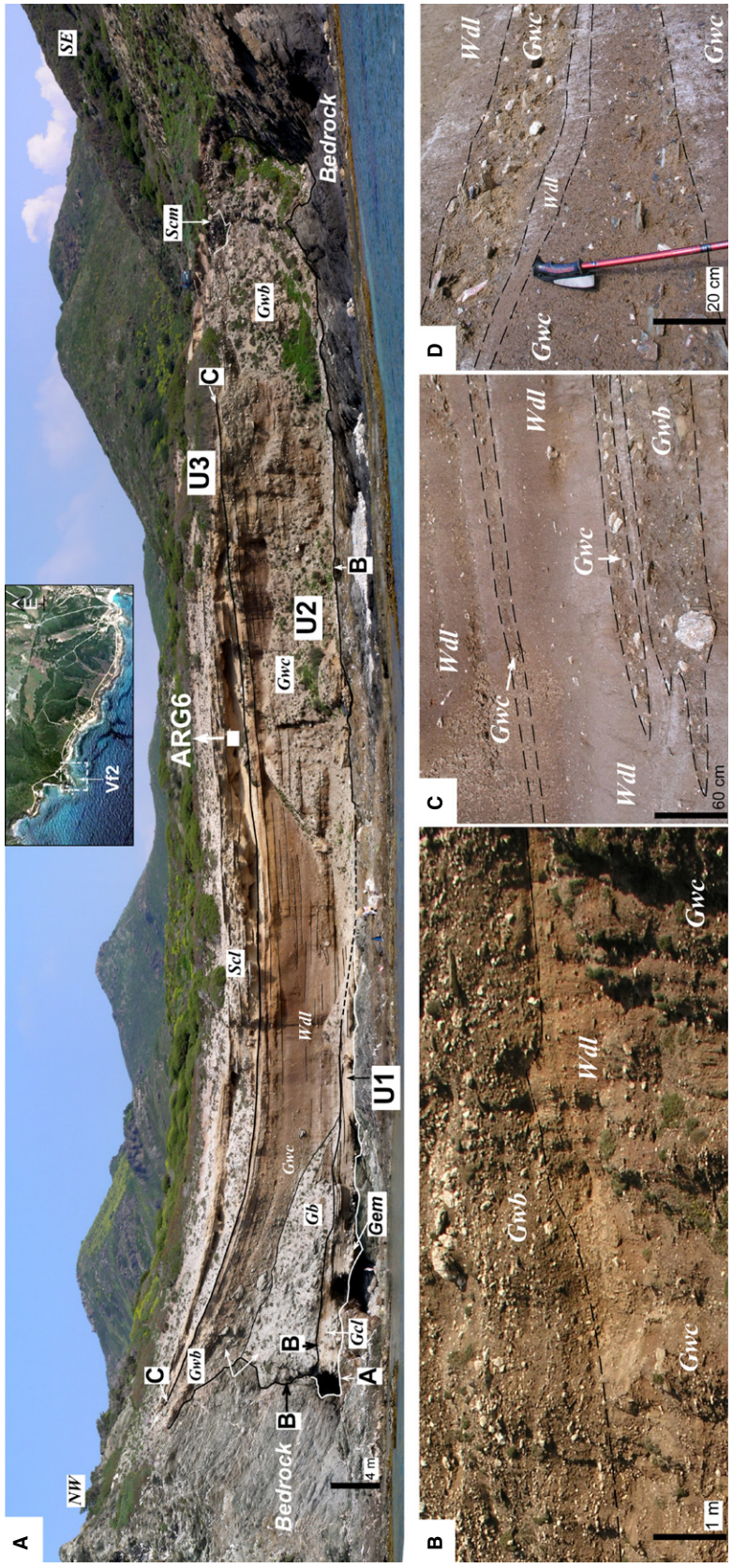


**Fig. 7.** (A) Panoramic view of the sedimentary succession filling up the valley/cove fill area Vf2 with inset location map. From the bottom up: marine deposits of Unit U1 (on the left side resting on bedrock) overlain by debris-flow dominated alluvial fan deposits (Unit U2), capped by sandy bodies of U3. Note that on the left side of the picture there is a talus cone (facies 'Gb'). Key for facies is in Table 1. The white square indicates the sample position for optically stimulated luminescence dating. (B) Conglomeratic debris-flow deposits with variable clast sizes ('Gwb' and 'Gwc') and reddish silty matrix. (C) Bouldery debris-flow deposit 'Gwb' capped by an alternation of siltstone 'Wdl' and conglomeratic debris-flow 'Gwc' deposits. (D) Alternating conglomeratic 'Gwc' and siltstone 'Wdl' debris-flow deposits.

palaeosol layer, 80 cm thick and variably eroded, composed of dark reddish brown (5 YR 3/6), massive, siltstone with disseminated angular pebbles and root bioturbation.

Unit U2a deposits have been interpreted as debris-flow deposits with various amounts of fine matrix. Some thin, fine-grained layers may be indicative of water winnowing during the latest stages of the sediment gravity flow events. Moreover, variation in particle sizes in various parts of the system and local channelization may be associated with lateral switching of the feeding flows. The upper U2b unit is more gravelly and better structured than the lower Unit U2a (Fig. 6D). Locally it shows large cut and fill structures with floors armoured by a single level of vein-quartz cobbles or pebbles (Fig. 6B and D).

The overall deposition of coarser deposits (U2b) over finer strata (U2a) may indicate outward progradation of a fan system still dominated by debris flow but acquiring an increased contribution of water-flow deposits in the upper unit. The palaeosol separating the two units may record either a decrease in the rate of sediment supply associated with overall climatic conditions, or lateral switching of the uphill feeding stream mouth. Local switching and reactivation of the streams crossing the fan were responsible for the relatively deep channel cuts into the palaeosol layer (Fig. 6D). Similarly, switching of some ephemeral creeks crossing the fan may have generated the cut and fill structure of Unit U2b.

The fill of the smaller cove Vf2 is superbly exposed quasi-perpendicular to the direction of the main sedimentary input (Figs 2A and 4 – Logs 8 to 12 and 7A). The depositional architecture of U2 (not separable into U2a and U2b) is similar to that of Vf1. There is a core/apex area characterized by chaotic silty cobble/boulder conglomerates (facies Gwb) near the valley stream entrance (right side of Fig. 7A). This area grades laterally into boulder and cobble layers (Gwc) interbedded with thin pebbly silty deposits (Fig. 7B) and, distally (central-left side of Fig. 7A), into a sequence of rhythmically alternating, poorly sorted, massive siltstone layers (Wdl) with a variety of dispersed pebbles and some cobbles, and thinner lensing silty conglomerate (Gwc). Locally nose-like gravelly layers (Gwb/Gwc) are interbedded with predominantly silty deposits (Fig. 7C and D). These deposits were formed primarily by debris flows, coarse-grained in the core of the structure near the sediment injection point, changing into silty-rich debris-flow deposits in more distal parts.

The northernmost flank of the cove (far left side of Fig. 7A) is bounded by a high-vertical cliff exposing metamorphic bedrock. The cove fill near this contact consists of a fossiliferous, cobble-pebbly coastal storm deposit (Unit 1: Fig. 4) overlain by wedge-shaped, steeply inclined (up to 40°) conglomeratic lenses composed of quartz and metamorphic angular pebbles to boulders. The texture of these lenses varies from openwork to clast-supported with a moderate reddish brown fine-grained matrix (facies Gb). This conglomeratic body is interpreted to represent a talus cone dominated by rockfall deposits formed near the valley flank. The reddish matrix is interpreted to be of secondary origin due to a later 'wash-in' of finer material derived from uphill soils during the debris-flow dominated fan migration. The talus cone deposits are progressively replaced upward by debris-flow deposits (facies Gwb/Gwc; Fig 7A).

Along the other depositional study areas (Al and PP), Unit U2 is again not consistently separable in to a lower and upper part. It is characterized by relatively thin (3 m thick maximum), mainly siltstone and minor conglomerate bodies (Figs 4 and 8). Fine-grained deposits are characterized by reddish brown (2·5 YR 5/4) laminated siltstone with angular pebbles aligned in layers and occasionally bioturbated by roots. These deposits are interpreted as partially pedogenized, wet debris flows (Fig. 8D). Locally decimetre-thick conglomeratic bodies in concave-upward lenses are most likely to be associated with very shallow channels (Fig. 8D). This sedimentary body represents fine-grained debris-flow deposits developed in the very distal area of alluvial systems (fan toes). The occasional gravelly layers are interpreted as channel deposits of small ephemeral creeks.

*Unit U3*

Unit U3, bounded at the base by a slightly erosive surface C, rests on debris-flow dominated deposits of Unit U2 (Fig. 4). This unit is mainly composed of relatively thick (8 m thick maximum) sandy and sandy-gravelly deposits. Unit U3 is interpreted to represent water-flow dominated alluvial fans, as demonstrated below.

In the Al1, Al2 and Al3 areas, Unit U3 is mainly composed of yellowish orange (7·5YR 7/8), poorly to fairly well-sorted, medium to

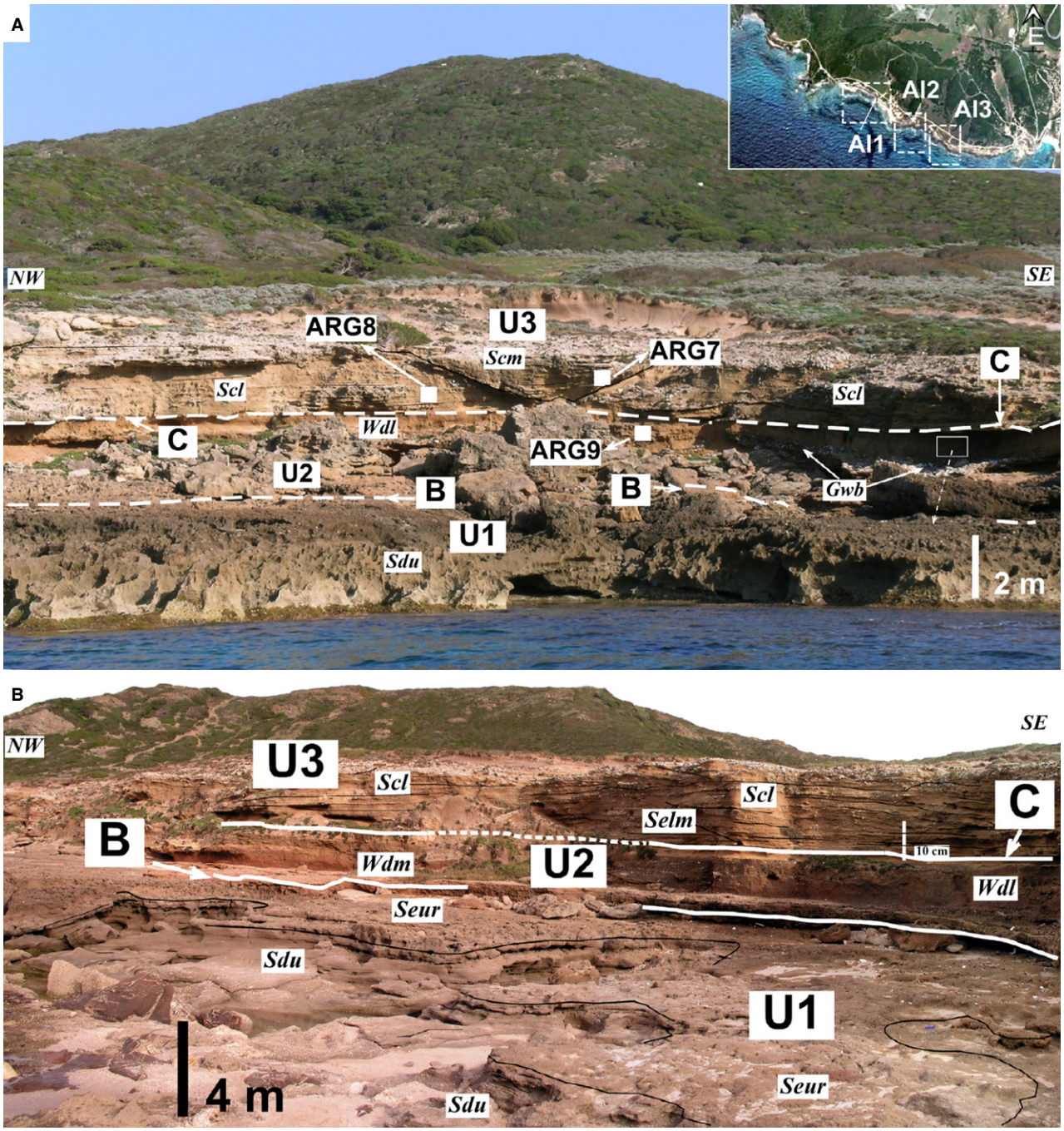


**Fig. 8.** (A) Panoramic and cross-section views of the water-flow dominated alluvial fan system Al2 with inset location map. From the bottom up: marine deposits (Unit U1), overlain by gravity-flow dominated sediments (U2) and capped by thick water-flow dominated fan deposits (U3). Note that there is a well-developed channel in the middle of the figure (2 m thick and 7 m wide) filled by sandy deposits of facies Scm over a thin basal pebbly lag. Key for facies is in Table 1. The white squares indicate the sample positions for optically stimulated luminescence dating. (B) Cross-section of alluvial fan Al1. From the bottom up: marine deposits of Unit U1 composed of well-sorted, laminated sandy-granule strata (Sdu) capped by highly bioturbated massive sandy deposits (Seur). Thick silty-pebbly debris-flow and palaeosol deposits (Wdl and Wdm) of U2 rest on the unconformity 'B' and are bounded at the top by unconformity 'C'. The succession is capped by water-flow dominated fan deposits of U3 composed of sandy/gravelly, laminated sheetflood deposits and channel fills (Scl and Scm). Key to facies is in Table 1.

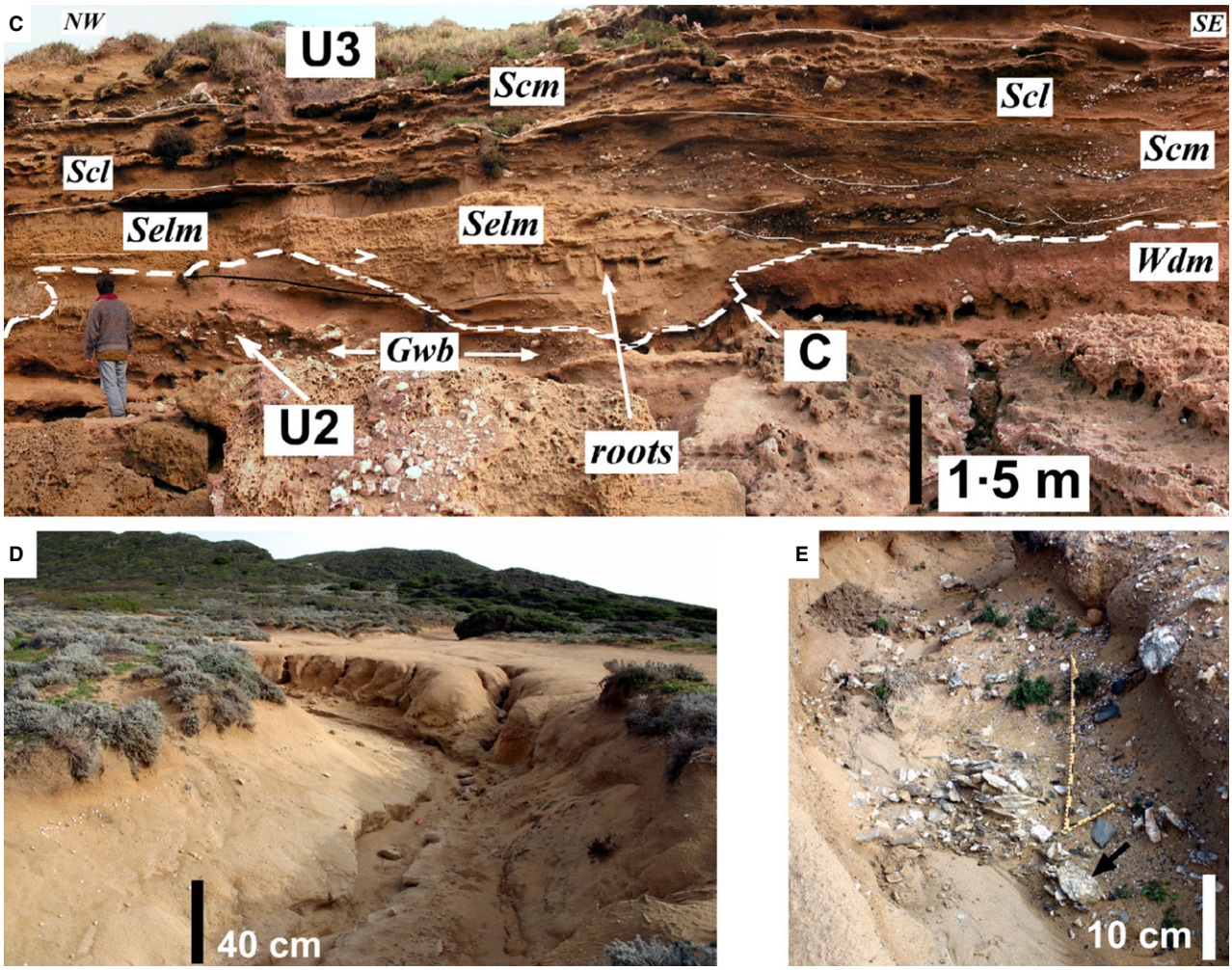


**Fig. 8.** (C) Cross-section of the water-flow dominated alluvial fan system Al3. Note at the base a highly eroded (unconformity 'C') gravity-flow dominated (U2) unit composed of thick silty-pebbly strata (Wdl), local gravelly debris-flow deposits (Gwb) and, on the right side, a palaeosol (Wdm) remnant. Water-flow dominated fan deposits of U3 cap the succession. Note the presence at the base of U3 of a massive aeolian sand sheet (Selm) deposit highly bioturbated by roots and locally eroded by thin sandy-gravelly channel fill deposits (Scm). Key for facies is in Table 1. (D) Modern rills and small channels on the surface of the alluvial fan. (E) Detailed view of the quartz-clast gravelly lag at the base of the modern channel of Fig. 8D.

coarse-grained sandstone with minor sandy conglomerate. The sandstone mainly consists (55% of total weight) of bioclastic fragments (such as red algae, molluscs, echinoids, benthic foraminifera and bryozoans) and minor (45% of total weight) siliciclastic grains (quartz, feldspar and phyllite fragments). Coarse clasts are angular to sub-angular pebbles and cobbles of metamorphic rocks (vein-quartz and phyllites). Some imbricated landward clasts occur as lag at strata boundaries or occasionally are disseminated in layers. The principal sedimentary structures consist of quasi-planar beds (inclined from 2° to 8° seaward approximately parallel to the fan depositional surface; facies Scl) and poorly stratified sandstone and/or sandy gravelly lenses forming channels of various dimensions (maximum 3 m deep and 6 m wide; facies Scm; Fig. 8). Cross-beds are rare to absent and sandstones are locally bioturbated by roots.

At present, the water-flow dominated fan areas (Al1, Al2 and Al3) are cut by rills and small channels with thin quartz-clast gravel lags (Fig. 8D and E). Based on Blair (1999b), non-catastrophic rainfall events produce partially confined flows that concentrate the erosion capacity in the fan area, creating rills and small channels with gravelly lags. A similar explanation is assumed here for channel fill deposits (facies Scm) of Unit U3.

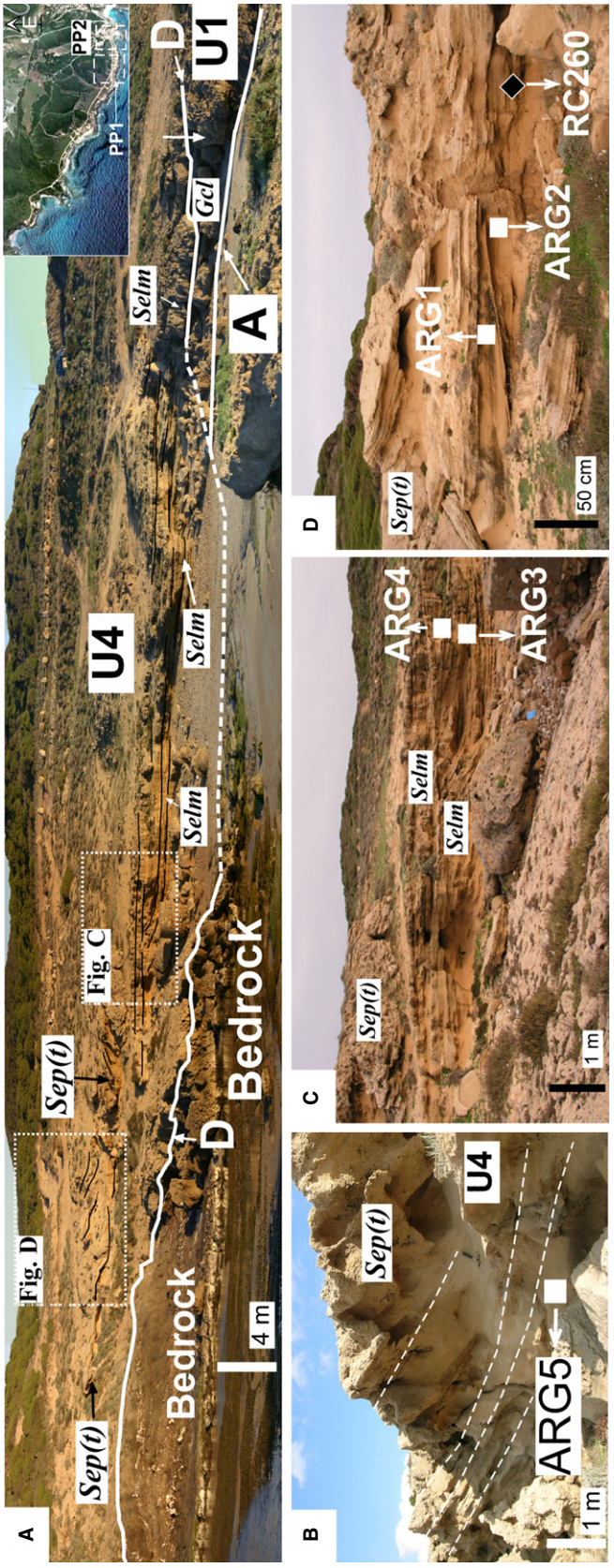


**Fig. 9.** (A) Panoramic view of the dunefield system developed at the base of the gently inclined hillslope in the PP2 area, with inset location map. Unit U4 rests directly on the bedrock (left side) and on deeply eroded (unconformity 'D') marine deposits (Sdu) of Unit U1 (right side; Key to facies is in Table 1). (B) Windblown deposit of Unit U4 at the hillslope area PP1. White square indicates the position of the optically stimulated luminescence(OSL) ARG5 sample. (C) Detailed view of the plane-bedded aeolian sand sheet deposits (Selm). White squares indicate the position of OSL samples. (D) Cross-bedded dune deposits [Sep(t)]. The white squares indicate the positions of samples for OSL dating and the black diamond indicates the position of a terrestrial gastropod shell used for radiocarbon dating.

A peculiar sedimentary body (facies Selm) crops out only on the Al3 area at the base of the unit (Figs 8C and 4 – Log. 24). This deposit is characterized by yellowish orange (10YR 8/6), fairly well-sorted, massive sandstone in layers up to 1 m thick. The medium to coarse-grained sands consist mainly of marine bioclasts (70% of total weight) and minor siliciclastic material (30% of total weight). Root traces are widespread and terrestrial gastropods occur locally. No bedrock-derived clasts were observed to be disseminated or aligned in strata, nor filling

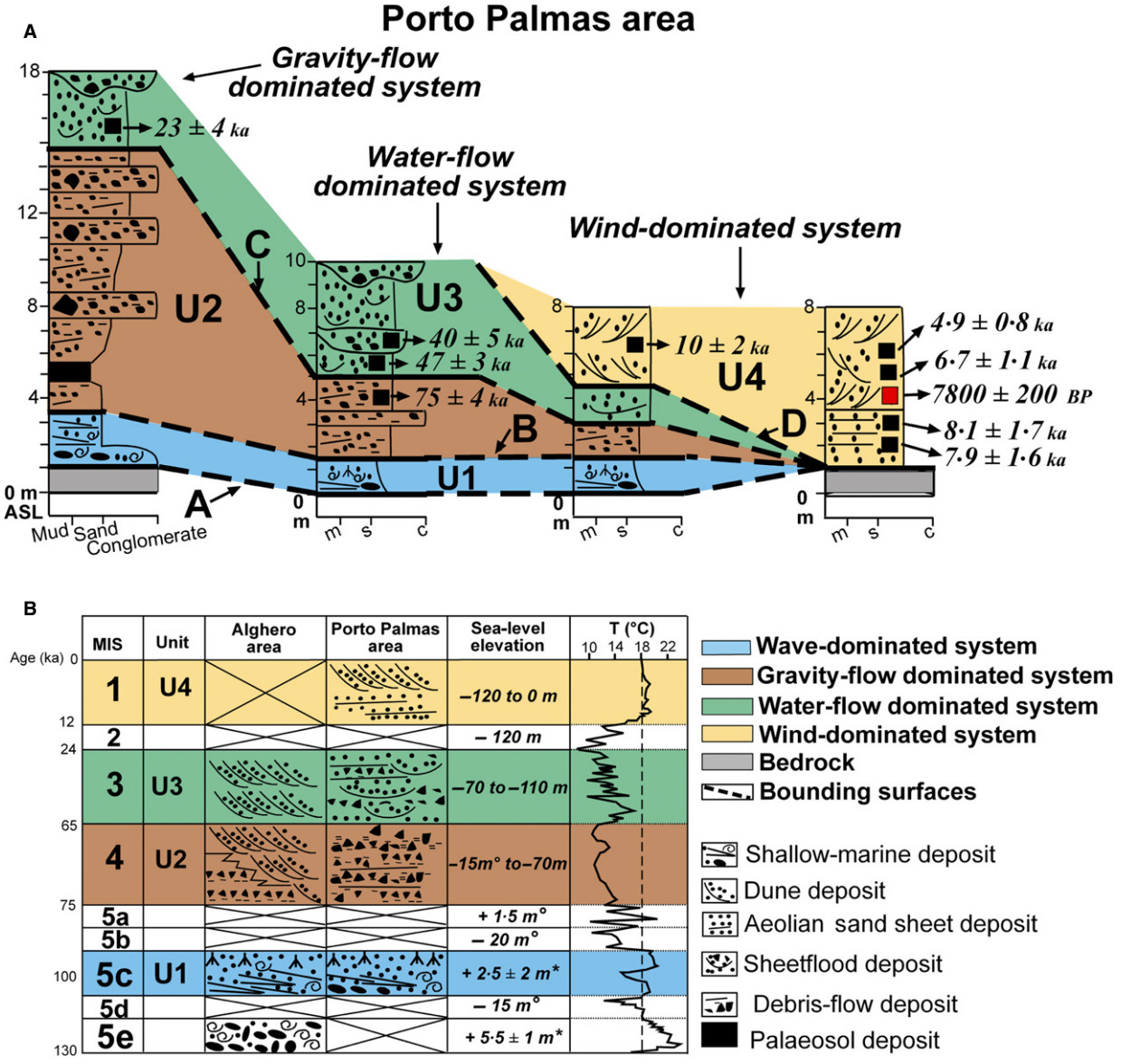


**Fig. 10.** (A) Schematic diagram showing the unconformity bounded units of the Porto Palmas area and their optically stimulated luminescence (OSL) and radiometric ages. Black squares correspond to the OSL ages obtained by quartz and/or K-feldspar analyses. The red square corresponds to the calibrated $^{14}C$ radiocarbon date (1$\sigma$ error; See Tables 2B and 3 for more details on ages). (B) Comparison of Upper Pleistocene to Holocene stratigraphic units of Alghero, defined by Andreucci *et al.* (2010) and those for the Porto Palmas site described here. Sea-level elevation modified from Waelbroeck *et al.* (2002) and Siddal *et al.* (2007); sea-level expected elevation * based on Andreucci *et al.* (2010) and ° based on Dorale *et al.* (2010). In the right column is the average sea-temperature of the West Mediterranean basin (Martrat *et al.*, 2004). The dashed line corresponds to the present-day average sea temperature calculated from the last 20 years data of measured at Porto Torres (APAT, 2010; see Fig. 1A for site location).

channel-like lenses. This sandy body is deeply eroded by facies Scl and Scm (Fig. 8C). Facies Selm is interpreted to represent remnant wind-blown accumulations (aeolian sand sheet) rapidly stabilized by vegetation and highly eroded (Aeolian pods; *sensu* Rodríguez-López *et al.*, 2010).

In the Al1, Al2 and Al3 areas, Unit U3 represents the progradation of a flattish (average 6°), alluvial fan system developed on a coastal area at the mouth of a relatively steeply inclined, small catchment (Figs 2C and 8A). The fan system is mainly dominated by unconfined water-flows of high capacity and competence formed during heavy rainfall events with frequent switching of shallow channelized flows. These flash flood events produced strong erosion of the catchment area and of the coalescent fan lobes but, due to the loss of lateral confinement, rapidly deposited down-valley, tabular sheet-flood bodies (facies Scl; Fig. 8B).

Along the valley fill depositional area (Vf1, Vf2 and Vf3), Unit U3 is characterized by the same facies stacking pattern of the water-flow dominated alluvial fans area (Al1, Al2 and Al3) but with a slightly coarsening upward trend. This may indicate a progradation of the alluvial system due to the reactivation of the mountain streams carrying mainly bedrock clasts (i.e. coarse material of facies Scm at top of the cliff of Fig. 7A). Along the hillslope area (PP1), Unit 3 is composed of thin (1·5 m thick maximum) tabular sheetflood (Scl) deposits indicating the southernmost limit of the water-flow dominated alluvial fan systems (fan toes).

*Unit U4*

Unit U4 lies unconformably over both the metamorphic bedrock and all the other stratigraphic units (surface D: Fig. 9A). This unit crops out only at the southernmost side of the coastal apron-fan system (areas PP1 and PP2: Fig.4).

Unit U4 is characterized by yellowish orange (10YR 8/6), well-sorted, medium to coarse-grained sandstone beds up to 2 m thick. The sand grains mainly consist of marine bioclasts (70 to 80% of total weight) and minor siliciclastic material (20 to 30% of total weight). The principal structures range from planar (facies Selm) to trough cross-beds, with foresets dipping 15° to 30° [facies Sep(t): Fig. 9]. Root traces are occasionally widespread and terrestrial gastropods occur locally (Fig. 3C).

Unit U4 represents a coastal dunefield system developed along a gently inclined hillslope (valley flank). The highly bioturbated sandstones are wind-blown accumulations (aeolian sand sheets) in places stabilized by vegetation, whereas cross-bedded units represents dune bodies migrating inland. At the valley flank (PP1) area, dune foresets show an average dip direction towards the south (N178°) indicating that dune slip faces migrate parallel to the hillslope orientation accordingly to the dominant wind coming from north/north–west (Andreucci *et al.*, 2010; Figs 1C and 2A). Instead, at the base (centre) of the valley, dune cross-bed orientations show a main dip direction towards the north–east (N80°) indicating that dunes migrate inland (landward) ascending the hillslope. It is most likely that the topography funnelled the wind forcing the sand drift towards the north–east. Moving downhill the topographical effect diminished and the dunefield migration was consistently to the south.

## CHRONOLOGY

A total of nine OSL sandy samples and one shell for radiocarbon dating were collected in the studied succession along the Porto Palmas apron fan system (Fig. 10A; Tables 2 and 3). One OSL sample (ARG9) was collected in a debris-flow deposit (facies Gwc) and dated using both the SAR procedure on quartz (Murray & Wintle, 2000) and the post-infrared stimulation SAR (post-IR IRSL) at high temperature (290°C) on K-feldspar grains (Buylaert *et al.*, 2012). Quartz-OSL analysis of the ARG9 sample gives a reliable age of 74 ± 9 ka. The post-IR IRSL (290°C) analysis on K-feldspar grains dated ARG9 to 75 ± 4 ka, confirming the age of the debris-flow deposit.

Three samples (ARG6 to ARG8) were collected in sheetflood and channel fill deposits (facies Scl and Scm) and were dated using both quartz and K-feldspar grains. Sample ARG6 has a reliable Quartz-OSL age of 23 ± 4 ka. No post-IR IRSL (290°C) analyses on K-feldspar grains were applied to this sample because post-IR IRSL (290°C) methodology is not reliable for '<30 ka' samples (Thiel *et al.*, 2011). Sample ARG7 has a Quartz-OSL age of 36 ± 4 and the K-feldspar post-IR IRSL (290°C) age is 43 ± 5 ka. However, both ages are within errors of each other, indicating an average of *ca* 40 ka. Sample ARG8 is quartz saturated, but the K-feldspar-post-IR IRSL (290°C) analysis provided a reliable age of 47 ± 3 ka.

Five samples (ARG1 to 5) were collected in aeolian deposits [facies Selm and Sep(t)] and have reliable Quartz-OSL ages of 4·9 ± 0·8 ka, 6·7 ± 1·1 ka, 7·9 ± 1·6 ka, 8·1 ± 1·7 ka and 10 ± 2 ka, respectively, with an average of *ca* 7·5 ka. The radiocarbon analysis, conducted on a shell collected in between samples ARG2 and ARG4, gives an age range between 8060 and 7675 BP (calibrated ± 1$\sigma$ error; Table 3, Fig. 3D), confirming the age of the aeolian strata.

## DISCUSSION

### Landscape evolution over the last 100 000 years

The sedimentary pattern of the Porto Palmas coastal apron-fan system greatly varied through time and space according to global factors, such as climatic changes and sea-level fluctuations, and to local elements, such as sediment type and supply and bedrock morphology. No data are available for Unit U1; however, the overlying debris-flow deposits have an age of at least 74 ka (Fig. 10A). Moreover, similar coastal deposits cropping out along the nearby Alghero area and at the same height of *ca* 1·5 m have OSL ages of 98 ± 8 ka and 97 ± 6 ka (Andreucci *et al.*, 2010). Therefore, the shallow-marine to coastal deposits of Unit U1 most probably developed during the last interglacial stage and are tentatively assigned to MIS 5c (*ca* 100 ka; Fig. 10B). The sedimentary evidence presented above indicates that the palaeogeography of the Porto Palmas area during MIS 5c was (and is now) characterized by a suite of gravelly or mixed sand and gravelly pocket beaches developed in coves between high cliffs or on a bedrock wave-cut platform with variable surface morphology. Locally in response to a north–west longshore current, sandy beaches prograded offshore and generated coastal bar/spit systems. The sea-level was *ca* 1·5 m above the present (Andreucci *et al.*, 2010; Dorale *et al.*, 2010) and the average sea-temperature of the West Mediterranean basin was *ca* 20°C (Martrat *et al.*, 2004); that is, similar to the present-day temperature measured along north-western Sardinia coasts (18 to 20°C; APAT, Agenzia per la Protezione dell'Ambiente per i servizi Tecnici, 2005, 2010).

The overlying Unit U2, based on the OSL age, is thought to have formed at the transition between MIS 5 and MIS 4 (*ca* 75 ka) when a rapid sea-level fall of *ca* −70 m (below the present sea-level) occurred (Waelbroeck *et al.*, 2002). As consequence of this fall, the coastline at Porto Palmas regressed *ca* 3 to 4 km from the present position (Figs 1C and 10B) and a debris-flow dominated fan system expanded offshore over the present-day shelf for at least 500 m. The average sea temperature dropped by *ca* 8°C from the temperature estimated for MIS 5c, and the climate significantly deteriorated from the previous warm sub-humid to humid conditions (Kindler *et al.*, 1997) becoming colder and semi-arid (Moreno *et al.*, 2012). Based on Nanson & Gibling (2003), dry system debris-flow dominated alluvial fans are considered typical of arid regions, and are activated by occasional strong rainstorms favouring gravity-flow processes along sparsely vegetated valley flanks (Hampton & Horton, 2007; Cannon *et al.*, 2008; Morton *et al.*, 2008). The rainstorms would have favoured the formation of debris flows that removed the deep soils probably formed along the hill flanks during the humid, warm MIS 5. This interpretation is supported by the extensive reddish-brown, fine-grained deposits found in the fans at the coast.

Similar mechanisms of fine material production and transport were proposed for reworked palaeosol strata of similar age (*ca* 70 ka) that crop out in the nearby Alghero area (Andreucci *et al.*, 2012). This interpretation is further supported by evidence of erosion and colluviation of weathered MIS 5 materials during the beginning of the MIS 4 glacial phase reported for palaeosol sequences in Tuscany, Central Italy (Mirabella *et al.*, 1992), south–east Spain and Mallorca (Ortiz *et al.*, 2002; Muhs *et al.*, 2010). Moreover, a minor amount of reddish, fine-grained material deposited during this period may have been associated with the iron-rich dust that, like today, blows from the Sahara Desert (Genova *et al.*, 2001).

Unit U3 is OSL dated to MIS 3 (*ca* 65 to 24 ka). This stage is characterized by variable sea-level fluctuations from −70 to −50 m below the present sea-level (bsl) reaching a final elevation −110 m (bsl) at 24 ka (Waelbroeck *et al.*, 2002; Siddal *et al.*, 2007), which is thought to correspond to a coastline regression of *ca* 5 km seaward of present (Fig. 1C). As a consequence of this regression, the water-flow dominated fan system expanded offshore over the present-day shelf for at least 1 km. Sea temperature fluctuated during this stage with warming Dansgaard–Oeschger (D/O) cycles and cooling Heinrich (H)

events, but at the very end of MIS 3 temperature had dropped at least 12°C compared with MIS 5c (Fig. 10B; Martrat *et al.*, 2004). Temperature variations associated with the D/O and H events triggered millennial time scale reorganisations of precipitation distribution that were responsible for alternating phases of aridity and humidity during MIS 3 (Rahmstorf, 2002; Hubber *et al.*, 2006).

The MIS 3 alluvial fans are characterized by a double sediment source. Material derived in variable amounts from the bedrock (conglomerate metamorphic rocks) of the inland hills and from the marine bioclastic sands of the shelf. Nowadays, along the Porto Palmas coast, a major amount of sand is stored in the sea grass meadow at a depth of −14/−30 m (bsl) and only occasionally on small sandy-gravelly pocket beaches (Fig. 1C). It is possible to infer that much of the bioclastic sand preserved in the alluvial fans was generated in a similar environment during the last interglacial stage (MIS 5), when the sea-level was the same or higher than at present and the coastline was similar to the modern one (Andreucci *et al.*, 2010; Dorale *et al.*, 2010). Moreover, the carbonate factory producing bioclastic sand was active also during MIS 4 and MIS 3 but located seaward of the MIS 5 position because of sea-level regression. A reasonable inference to explain the high percentage of bioclasts in alluvial fan deposits is that during MIS 3, under variable sea-level elevations (hence coastline positions), bioclastic marine sand was exposed and blown inland from the shelf over the apron fan system to form extensive aeolian sand sheet deposits (arid phases). Subsequently, during humid phases, it is suggested that these aeolianites were rapidly stabilized by vegetation and that catastrophic rainfall events triggered flash floods in the catchment area that flowed over the coastal plain. These floods transported siliciclastic sediments from the catchment area, reworked the bioclastic aeolian sands and generated pebbly-sandy sheetflood deposits and sandy-gravelly channel fills in the fan lobes. Therefore, the water-flow dominated fans are characterized by a mixing of inland metamorphic clasts and marine sands (Fig. 8).

The available OSL ages indicate that these sedimentary processes may have continued for most of MIS 3 and, in particular, at *ca* 47 ka, 40 ka and 23 ka. Besides seasonal, annual and submillennial variations in the distribution of precipitation responsible for minor flash flood events, main fan lobe developments can be tied with Dansgaard–Oeschger (D/O) cycles. The available ages approximate those of some D/O events and, in particular, D/O 13 (*ca* 47 ka), D/O 8 (*ca* 39 ka) and D/O 2 (*ca* 23 ka; Hinnov *et al.*, 2002; Rahmstorf, 2002).

The climate along the north–western coast of Sardinia during the last glacial stage (MIS 2, *ca* 24 to 12 ka) was relatively cold and dry and the sea temperature had dropped at least 13°C from that during MIS 5c (Fig. 10B; Martrat *et al.*, 2004; Kuhlemann *et al.*, 2008). This stage was characterized by the maximum sea-level regression, with a sea-level drop of -120 m below the present sea-level (Waelbroeck *et al.*, 2002; Siddal *et al.*, 2007) that tentatively corresponds to a coastline regression of at least 7 to 8 km seaward of present. None of the deposits observed in the study area are clearly referable to MIS 2. This may be due to the limited number of dates available or to the thinness of the MIS 2 deposits preserved after the Holocene transgression reworking.

Unit U4 is characterized by aeolian sand sheets and coastal dunes dated to the early and middle Holocene (MIS 1; *ca* 10 to 4 ka). This stage involved a rapid sea-level transgression and a significant global climatic change (Waelbroeck *et al.*, 2002). The average sea-temperature increased at least 10°C compared with the Last Glacial Maximum (LGM), reaching the modern value of about 18°C (Martrat *et al.*, 2004). The U4 deposits, mainly composed of marine bioclastic fragments, indicate that during the Holocene transgression marine sands were progressively moved landward and blown inland to build up a coastal dunefield. Data from the nearby Grotta Verde cave (Antonioli *et al.*, 1994; Fig. 1B) indicate that 7000 years ago (corresponding to the approximate average age of the Porto Palmas dunes) sea-level was at least 10 m below present and this corresponds to a palaeo-shoreline about 100 m seaward (Fig. 1C). Nowadays at the southernmost site of the study area (PP2) a small pocket beach is backed inland by a low cliff carved on the Holocene aeolianites indicating an ongoing active coastline transgression (Fig. 9A).

## Accommodation space, sediment aggradation and valley entrenchment of alluvial fan systems

It is a well-recognized fact that accommodation space is provided by progressive subsidence of

the basin depocentre and this may lead to a thick deposition if the sediment supply is sufficiently large (Posamentier & Vail, 1988; Muto & Steel, 2000). However, the accommodation space in alluvial fan systems is also controlled by allogenic elements, such as tectonic uplift of the mountain range and sea-level rise (Shanley & McCabe, 1994; Viseras *et al.*, 2003). Moreover, for river-incised valley systems, it has been demonstrated that aggradation occurs during high sea-level stands and that stream entrenchment occurs during marine regressions (Calvache *et al.*, 1997; Viseras *et al.*, 2003; Catuneanu, 2006; Mattheus & Rodriguez, 2011). In particular, valley incision which normally starts from the shelf edge migrates upstream (landward) for tens to hundreds of kilometres eroding almost completely the preceding highstand shoreline (Boyd *et al.*, 2006).

The overall Porto Palmas coastal-apron fans (Unit U2) were developed along a tectonically stable area, with very low subsidence rates (0·01 mm $a^{-1}$). The ages presented above allow the present authors to infer that fans developed during a phase of forced regression (*sensu* Catuneanu, 2006) with a sea-level fall of at least 70 m. In this regional context, fluvial entrenchments (incised-valley formation) rather than alluvial fan aggradation would be expected. However, Catuneanu (2006) observed that the processes of aggradation or erosion were strongly linked to the balance between fluvial and/or marine erosion (energy flux) and sediment supply (mainly fluvial discharge). Thus, aggradation occurs only where sediment supply outpaces energy flux, and erosion occurs only where energy outpaces sediment load. Clear evidence that the small creeks active at Porto Palmas during the forced regression did not posses enough energy (erosional capability) to remove all the deposits and form an entrenched valley, is the presence at the base of the studied succession of the preceding highstand marine deposits (Unit U1; Fig. 4). Thus, the sediment load during the forced regression exceeded the erosional capacity of the small creeks, inducing an alluvial fan aggradation during the falling stage. Sediment was supplied from the large amount of soil developed during the previous MIS 5 interglacial and fine-grained sediments stored in the feeding valleys. Climatic deterioration reduced the vegetation cover and triggered valley flank denudation and sediment remobilization inducing the alluvial fan aggradation. Thus, sedimentation was mainly climate driven. Therefore, the Porto Palmas MIS 4 fan system highlights that, in local circumstances, climate can promote deposition despite falling sea-level during a glacial stage. Similar examples, where fluvial aggradation occurred during a glacial period, are reported from Quaternary deposits in Canada, the US Gulf Coast and Australia (Catuneanu, 2006; Sloss *et al.*, 2009).

The boundary between MIS 4 and MIS 3 is characterized by the lateral and vertical juxtaposition of sheetflood dominated alluvial (Unit U3) fans over the debris-flow (Unit U2) deposits. Besides the geomorphology of the basins, differences in source material were a key element influencing deposit characteristics. Similar observations have been made by several authors, including Blair (1999a,b,c) and Nichols & Thompson (2005). In particular, Blair & McPherson (1995) indicated that a change in the bedrock lithology of the fan drainage system was accompanied by the switching from a debris-flow dominated to a water-flow dominated deposit. In the current study the switch consisted of replacement of material sourced from inland bedrock with an overwhelming input of marine bioclastic sand blown from the partially open shelf, which mantled the coastal plain of the study area. Thus, it is worth noting that the source rock lithology did not change in the fan drainage system (catchment area), but changed in the alluvial fan zone.

The readily erodible bioclastic sands were reworked by partially channelized and sheetflows and mixed with some inland bedrock derived clasts in water-flow dominated alluvial fans. Therefore, the MIS 3 water-flow dominated sandy and sandy-conglomerate deposits (Unit U3) represent a dune-sourced alluvial fan system (Sweeney & Loope, 2001). Modern examples of dune-sourced sand reworked into water-flow dominated alluvial fans have been reported from continental and coastal settings where dunes are stabilized by vegetation, such as Nebraska, USA (Sweeney & Loope, 2001), the Netherlands (Jungerius & van der Meulen, 1988; Jungerius & Dekker, 1990), Brazil (Bigarella, 1975), Niger (Talbot & Williams, 1978, 1979) and Australia (Bridge & Ross, 1983; Thompson, 1983).

A comprehensive investigation of the dune-sourced alluvial fan deposits of the Nebraska Sand Hills (USA) conducted by Sweeney & Loope (2001) revealed that typical deposits are laminated sands (interpreted as sheetflood deposits), unstructured sands (identified as hy-

perconcentrated flow deposits) and sandy trough cross-strata (interpreted as channel fills). The Nebraska Sand Hills alluvial fans possess an average height of 10 m and a slope inclination of 8·5°; that is, comparable to those measured at the Porto Palmas study sites. The overland flows triggered by intense rainfall are necessary for sand mobilization and transport from the dunes to the alluvial fan surface. Based on Sweeney & Loope (2001), in order to initiate rill and gully formation on dunes it is necessary to reduce the sand hydraulic conductivity (infiltration) with vegetation (grass-stabilization of dune crests) and surface crusts. The studied alluvial fan deposits show clear evidence of dune-stabilization by vegetation (Fig. 8D); conversely, no surface crusts have been observed. However, several examples from the modern and ancient rock records (Svendsen *et al.*, 2003; Rodríguez-López *et al.*, 2010) have reported that water flows generated on relatively steeply inclined slopes (composed of low-hydraulic conductivity bedrock) possess enough energy to erode dunes, even if their crests are not covered by crusts. A similar explanation is assumed for the Porto Palmas deposits.

Several examples of the interaction between water flows and sand dunes are well-known in the literature with fluvial-like deposits (for example, overbank-deposits, laminated sandy strata and fluvial channel deposits) in the interdune areas of flattish desert and coastal environments or pebble–cobble-sand sheetflood, sand bedload, debris-flow and hyperconcentrated flow deposits in desert margin environments where fan toes reach the outer erg system (Langford, 1989; Langford & Chan, 1989; Fryberger, 1991; Loope *et al.*, 1998, 1999; Scherer *et al.*, 2007; Jordan & Mountney, 2010; Rodríguez-López *et al.*, 2010). There are several examples in the rock record of dune-alluvial fan interactions in coastal settings, mainly from the Uppermost Pleistocene deposits of south–east Australia (Gardner *et al.*, 2006) and the western Mediterranean (Fornós *et al.*, 2009; Andreucci *et al.*, 2010). Those authors suggested that marine generated carbonate aeolianites mantling coastal areas were partially reworked by water flows, supporting the interpretation proposed for the deposits studied here. However, documented interactions occurred over short time intervals (a few thousand years; Gardner *et al.*, 2006) and/or in peculiar and restricted areas, such as on sand ramps near vertical coastal cliffs (Fornós *et al.*, 2009; Andreucci *et al.*, 2010), without completely dismantling the dunefield system. Conversely, at Porto Palmas this interaction was active for at least 20 000 years, building a relatively thick dune-sourced alluvial fan system on a gently sloping coastal plain and involving almost complete reworking of a dunefield. Moreover, the dune-sourced alluvial fan deposits of Porto Palmas (Unit U3) can be associated with a phase of bioclastic-rich aeolianite formation in the western Mediterranean region during glaciation (El-Asmar & Wood, 2000; Brooke, 2001; Nielsen *et al.*, 2004; Le Guern & Davaud, 2005; Fornós *et al.*, 2009; Andreucci *et al.*, 2010; Elmejdoub *et al.*, 2011). Overall, The Porto Palmas fan systems are broadly similar in type and age to those on Crete and in west Anatolia (Nemec & Postma, 1993; Nemec & Kanzaci, 1999), suggesting a west to east Mediterranean correlation of the main climatic events.

## CONCLUSIONS

This study of the coastal apron-fan system of the Porto Palmas area of north–western Sardinia has shed light on the palaeoenvironmental evolution of complex coastal areas of the central western Mediterranean during the Late Pleistocene–Holocene.

**1** The studied sedimentary sequence is composed of debris-flow dominated alluvial fans, water-flow dominated alluvial fans and coastal dunes. These occur over sand and gravel beach deposits (Unit U1), possibly deposited during the last interglacial [Marine Isotope Stage (MIS) 5c; *ca* 100 ka].

**2** Based on optically stimulated luminescence (OSL) and radiometric data, the sediment gravity-flow dominated systems (Unit U2) were developed during a sea-level regression that occurred at the beginning of the glacial phase (MIS 4; 75 to 65 ka). The water-flow dominated alluvial fans (Unit U3) record MIS 3 (65 to 23 ka) and, finally, the wind-blown dominated deposits (Unit U4) developed during the Holocene (MIS 1; 10 to 5 ka).

**3** Bedrock morphology has been critical in controlling the sediment accumulation space within the study area. The basal marine deposits were developed on a bedrock platform and have mostly been preserved in cliff-sheltered coves. The presence of narrow, steep valleys and coves allowed the formation of debris-flow dominated alluvial fan systems. Conversely, on wider and

flatter coastal planes, floods could expand, rework sediments and build up water-flow dominated fans.

**4** The composition and structure of debris-flow and water-flow dominated alluvial systems partly reflect changes through time of the sediment source. Material sourced from inland bedrock built up relatively thick debris-flow dominated alluvial fans (Unit U2; MIS 4). This material was partially replaced during MIS 3 by the overwhelming input of marine, bioclastic, wind-blown sand from the exposed shelf (Unit U3). Near the bedrock source, the different lithological inputs (inland bedrock and shelf bioclastic sand) alternated and with additional reworking in water-dominated fans repetitive stratigraphic deposits developed. Moreover, this change in lithology occurred directly in the coastal plain, where the active fan lobes extended, and not in the catchment area as in previously described examples.

**5** Local and global climatic variations, together with global sea-level fluctuations strongly influenced the sediment accumulation patterns.

During the MIS 4 forced regression, the climatic and local geomorphology promoted a debris-flow dominated fan aggradation rather than a complete exhumation of coastal valleys and coves in the Porto Palmas area. The MIS 4 climatic deterioration led to a progressive disruption of inland vegetation cover and to repeated denudation of weathered materials stored along the valleys of short streams. As a result, sediment supply outpaced the fluvial energy capable of significant valley incision and significant removal of coastal deposits. Thus, in local circumstances alluvial fans can aggrade and prograde even during sea-level regression.

During the MIS 3 regression, up to 2·5 km of the shallow western shelf of Sardinia became exposed and a new source of sediment was opened: shallow marine bioclastic sands. Rapid climatic fluctuations controlled the sedimentation trend. It is likely that aeolian dunes and sand sheets were formed throughout the shelf, particularly during drier phases. Some enhanced, more frequent stream-flows may have reworked bedrock-derived material and wind-blown bioclastic sands near the coastal highlands (present coastal hills), forming water-flow dominated alluvial fans during wetter phases, possibly in response to wet/arid Dansgaard–Oeschger (D/O) cycles. The D/O events tentatively associated with the development of the main fan lobes are D/O 13 (*ca* 47 ka), D/O 8 (*ca* 39 ka) and D/O 2 (*ca* 23 ka). During the Holocene transgression (about 100 m in 10 ka) bioclastic sands were progressively moved landward and blown inland to build up a coastal dunefield in the southernmost part of the study area.

In conclusion, despite the thinness of the deposits, the Porto Palmas study area is one of the few coastal sites where almost all of the main climatic fluctuations that occurred during MIS 4 and MIS 3 are recorded in the sedimentary record and can be used for West to East Mediterranean correlation.

## ACKNOWLEDGEMENTS

We are indebted to Roberta Ceravola and Lorenzo Angeletti for field assistance. We thank the Journal Editor Stephen Rice, the Associate Editor Mariano Marzo and the reviewers Mark Sweeney and Cesar Viseras for pushing the authors to extract the best from their observations and for insightful comments which greatly improved this manuscript. IPM disassociates himself from the dune-sourced interpretation. Financial support: to SA was provided by a young researcher grant from Regione Autonoma Sardegna: PO Sardegna FSE 2007–2013 and L.R. 7⁄2007 *Promozione della ricerca scientifica e dell'innovazione tecnologica in Sardegna* (resp. Stefano Andreucci); to IPM by a visiting professorship granted from the University of Sassari (resp. Vincenzo Pascucci); to VP by FAR (Fondo di Ateneo per la Ricerca, resp. Vincenzo Pascucci).

## REFERENCES

**Aitken, M.J.** (1985) *Thermoluminescence Dating*. Academic Press, London, 267 pp.

**Andreucci, S.**, **Clemmensen, L.B.**, **Murray, A.** and **Pascucci, V.** (2010) Middle to late Pleistocene coastal deposits of Alghero, northwest Sardinia (Italy): chronology and evolution. *Quatern. Int.*, **222**, 3–16.

**Andreucci, S.**, **Bateman, M.D.**, **Zucca, C.**, **Kapur, S.**, **Akşit, İ.**, **Dunajko, A.** and **Pascucci, V.** (2012) Evidence of Saharan dust in upper Pleistocene reworked palaeosols of northwest Sardinia, Italy: palaeoenvironmental implications. *Sedimentology*, **59**, 917–938.

**Antonioli, F.**, **Ferranti, L.** and **Lo Schiavo, F.** (1994) The submerged neolithic burials of the Grotta Verde at Capo Caccia (Sardinia, Italy). Implication for the Holocene sea-level rise. *Mem. Descr. Carta Geol. d'Ital.*, **52**, 329–336.

**APAT, Agenzia per la Protezione dell'Ambiente per i servizi** Tecnici (2005) Atlante delle coste: Il moto ondoso a largo delle coste italiane. Dipartimento Tutela delle acque interne e marine, Servizio difesa delle coste. Istituto

poligrafico e zecca dello stato, Roma. Available at: http://www.apat.gov.it/site/it-IT/Servizi_per_l'Ambiente/Stato_delle_coste/Atlante_delle_coste.

**APAT, Agenzia per la Protezione dell'Ambiente per i servizi** Tecnici (2010) Rete Ondametrica Nazionale. Available at: http://www.idromare.com (accessed November 2010).

**Armitage, S.J.**, **Duller, G.A.T.** and **Wintle, A.G.** (2000) Quartz from Southern Africa: sensitivity changes as a result of thermal pre-treatment. *Radiat. Meas.*, **32**, 571–577.

**Bateman, M.D.**, **Boulter, C.H.**, **Carr, A.S.**, **Frederick, C.D.**, **Peter, D.** and **Wilder, M.** (2007) Detecting Post-depositional sediment disturbance in sandy deposits using optical luminescence. *Quatern. Geochronol.*, **2**, 57–64.

**Bell, W.T.** (1979) Attenuation factors to absorbed dose in quartz inclusions for thermoluminescence dating. *Ancient TL*, **8**, 2–13.

**Bigarella, J.J.** (1975) Structures developed by dissipation of dune and beach ridge deposits. *Catena*, **2**, 107–152.

**Blair, T.C.** (1999a) Sedimentary processes and facies of the waterlaid Anvil Spring Canyon alluvial fan, Death Valley, California. *Sedimentology*, **46**, 913–940.

**Blair, T.C.** (1999b) Sedimentology of the debris-flow-dominated Warm Spring Canyon alluvial fan, Death Valley, California. *Sedimentology*, **46**, 941–965.

**Blair, T.C.** (1999c) Cause of dominance by sheet-flood vs debris-flow processes on two adjoining alluvial fans, Death Valley, California. *Sedimentology*, **46**, 1015–1028.

**Blair, T.C.** and **McPepherson, P.** (1995) Quaternary alluvial fans of southwestern Crete: sedimentation processes and geomorphic evolution. *Sedimentology*, **42**, 531–549.

**Blikra, L.H.** and **Nemec, W.** (1998) Postglacial colluvium in western Norway: depositional processes, facies and paleoclimatic record. *Sedimentology*, **45**, 909–959.

**Bluck, B.J.** (1967) Sedimentation of beach gravels: examples from South Wales. *J. Sed. Petrol.*, **37**, 128–156.

**Bøe, A.G.**, **Murray, A.** and **Dahl, S.O.** (2007) Resetting of sediments mobilised by the LGM ice-sheet in southern Norway. *Quatern. Geochronol.*, **2**, 222–228.

**Boyd, R.**, **Dalrymple, R.W.** and **Zaitlin, B.A.** (2006) Estuarine and incised-valley facies models. In: *Facies Models Revisited* (Eds H.W. Posamentier and R.G. Walker), *SEPM Spec. Publ.*, **84**, 171–235.

**Bridge, B.J.** and **Ross, P.J.** (1983) Water erosion in vegetated sand dunes at Cooloola, south-east Queensland. *Ann. Geomorphol.*, **45**, 227–244.

**Bronk Ramsey, C.** (2009) Bayesian analysis of radiocarbon dates. *Radiocarbon*, **51**, 337–360.

**Brooke, B.** (2001) The distribution of carbonate aeolianite. *Earth-Sci. Rev.*, **55**, 135–164.

**Buylaert, J.P.**, **Vandenberghe, D.**, **Murray, A.S.**, **Huot, S.**, **De Corte, F.** and **Van den Haute, P.** (2007) Luminescence dating of old (>7 ka) Chinese loess: a comparison of single-aliquot OSL and IRSL techniques. *Quatern. Geochronol.*, **2**, 9–14.

**Buylaert, J.P.**, **Murray, A.S.**, **Thomsen, K.J.** and **Jain, M.** (2009) Testing the potential of an elevated temperature IRSL signal from K-feldspar. *Radiat. Meas.*, **44**, 560–565.

**Buylaert, J.-P.**, **Jain, M.**, **Murray, A.S.**, **Thomsen, K.J.**, **Thiel, C.** and **Sohbati, R.** (2012) A robust feldspar luminescence dating method for Middle and Late Pleistocene sediments. *Boreas*, **41**, 435–451.

**Calvache, M.L.**, **Viseras, C.** and **Fernández, J.** (1997) Controls on fan development - evidence from fan morphometry and sedimentology, Sierra Nevada, SE Spain. *Geomorphology*, **21**, 69–84.

**Cannon, S.H.**, **Gartner, J.E.**, **Wilson, R.C.**, **Bowers, J.C.** and **Laber, J.L.** (2008) Storm rainfall conditions for floods and debris flows from recently burned areas in southwestern Colorado and southern California. *Geomorphology*, **96**, 250–269.

**Carmignani, L.**, **Barca, S.**, **Oggiano, G.**, **Pertusati, PC.**, **Salvadori, I.**, **Conti, P.**, **Eltrudis, A.**, **Funedda, A.** and **Pasci, S**. (2001) Geologia della Sardegna: note illustrative della Carta Geologica della Sardegna a scala 1:200.000. *Mem. Descr. Carta Geol. Ital.*, **60**, 240 pp. Istituto poligrafico e zecca dello stato, Roma.

**Catuneanu, O.** (2006) *Principles of Sequence Stratigraphy*. Elsevier, Amsterdam, 376 pp. ISBN 978-0-444-51568-1

**Chamyal, L.S.**, **Khadkikar, A.S.**, **Malik, J.N.** and **Maurya, D.M.** (1997) Sedimentology of the Narmada alluvial fan, western India. *Sed. Geol.*, **107**, 263–279.

**Coltorti, M.**, **Melis, E.** and **Patta, D.** (2010) Geomorphology, stratigraphy and facies analysis of some Late Pleistocene and Holocene key deposits along the coast of Sardinia (Italy). *Quatern. Int.*, **222**, 16–30.

**Delitala, A.M.S.**, **Cesari, D.**, **Chessa, P.A.** and **Ward, M.N.** (2000) Precipitation over Sardinia (Italy) during the 1946-1993 rainy seasons and associated large-scale climate variations. *Int. J. Climatol.*, **20**, 519–541.

**Doglioni, C.**, **Fernández, M.**, **Gueguen, E.** and **Sábat, F.** (1999) On the interference between early Apennines–Maghrebides back arc extension and Alps–Betics orogen in the Neogene Geodynamics of the Western Mediterranean. *Boll. Soc. Geol. Ital.*, **118**, 75–89.

**Donda, F.**, **Gordini, E.**, **Rebesco, M.**, **Pascucci, V**, **Mosetti, R.G.**, **Lazzari, P.** and **Fontolan, V.** (2008) Shallow water sea-floor morphologies around Asinara Island (NW Sardinia, Italy). *Cont. Shelf Res.*, **28**, 2550–2564.

**Dorale, J.A.**, **Onac, B.P.**, **Fornoś, J.J.**, **Gineś, J.**, **Gineś, A.**, **Tuccimei, P.** and **Peate, D.W.** (2010) Sea-level highstand 81,000 years ago in Mallorca. *Science*, **327**, 860–863.

**El-Asmar, H.M.** and **Wood, P.** (2000) Quaternary shoreline development: the northwestern coast of Egypt. *Quatern. Sci. Rev.*, **19**, 1137–1149.

**Elmejdoub, N.**, **Mauz, B.** and **Jedoui, Y.** (2011) Sea-level and climatic controls on Late Pleistocene coastal aeolianites in the Cap Bon peninsula, northeastern Tunisia. *Boreas*, **40**, 198–207.

**Ferranti, L.**, **Antonioli, F.**, **Mauz, B.**, **Amorosi, A.**, **Dai Pra, G.**, **Mastronuzzi, G.**, **Monaco, C.**, **Orrù, P.**, **Pappalardo, M.**, **Radtke, U.**, **Renda, P.**, **Romano, P.**, **Sansò, P.** and **Verrubbi, V.** (2006) Markers of the last interglacial sea-level high stand along the coast of Italy: tectonic implications. *Quatern. Int.*, **146**, 30–54.

**Fornós, J.**, **Clemmensen, L.B.**, **Gomez-Pujol, L.** and **Murray, A.S.** (2009) Late Pleistocene carbonate aeolianite deposits on Mallorca, western Mediterranean: a luminescence chronology. *Quatern. Sci. Rev.*, **28**, 2697–2709.

**Fryberger, S.G.** (1991) Unusual structures in the Oregon coastal dunes. *J. Arid Environ.*, **21**, 131–150.

**Funedda, A.**, **Oggiano, G.** and **Pascucci, V.** (2003) I depositi Miocenici della Sardegna settentrionale: il bacino del Logudoro. In: *Atti del Convegno GEOSED 2003* (Ed. V. Pascucci), pp. 381–414. Abstract book, Alghero, Italia.

**Gardner, T.W.**, **Webb, J.**, **Davis, A.G.**, **Cassel, E.J.**, **Pezzia, C.**, **Merritts, D.J.** and **Smith, M.B.** (2006) Late Pleistocene landscape response to climate change: eolian and alluvial fan deposition, Cape Liptrap, southeastern Australia. *Quatern. Sci. Rev.*, **25**, 1552–1569.

**Genova, N.**, **Meloni, S.**, **Oddone, G.M.** and **Melis, P.** (2001) On the origin of some red soils from Sardinia (Italy): a neutron activation analysis investigation. *J. Radioanal. Nucl. Chem.*, **2**, 355–360.

**Ginesu, S.**, **Derudas, A.**, **Enzo, S.**, **Secchi, F.** and **Sias, S.** (2009) The post-Tyrrhenian evolution in Sardinia: evidence from the Ebidozzi paleovallley (Argentiera, North-western Sardinia, Italy). *Geogr. Fis. Dinam. Quat.*, **32**, 23–30.

**Goodfriend, G.A.**, **Cameron, R.A.D.**, **Cook, L.M.**, **Courty, M.**, **Fedoroff, N.**, **Livett, E.** and **Tallis, J.** (1996) The Quaternary eolian sequence of Madeira: stratigraphy, chronology, and paleoenviromental interpretation. *Paleogeogr. Paleocl. Paleoecol.*, **120**, 195–234.

**Hampton, B.A.** and **Horton, B.K.** (2007) Sheetflow fluvial processes in a rapidly subsiding basin, Altipiano plateau, Bolivia. *Sedimentology*, **54**, 1121–1148.

**Hinnov, L.A.**, **Schultz, M.** and **Pascal, Y.** (2002) Interhemispheric space–time attributes of the Dansgaard–Oeschger oscillations between 100 and 0 ka. *Quatern. Sci. Rev.*, **21**, 1213–1228.

**Hubber, C.**, **Leuenberger, M.**, **Spahni, R.**, **Flückiger, J.**, **Schwander, J.**, **Stocker, T.F.**, **Johnsen, S.**, **Landais, A.** and **Jouzel, J.** (2006) Isotope calibrated Greenland temperature record over Marine Isotope Stage 3 and its relation to CH4. *Earth Planet. Sci. Lett.*, **243**, 504–519.

**Huntley, D.J.** and **Baril, M.R.** (1997) The K content of the K-feldspars being measured in optical dating or in thermoluminescence dating. *Ancient TL*, **15**, 11–13.

**Huntley, D.J.** and **Lamothe, M.** (2001) Ubiquity of anomalous fading in K-feldspars, and the measurement and correction for it in optical dating. *Can. J. Earth Sci.*, **38**, 1093–1106.

**Jordan, O.D.** and **Mountney, N.P.** (2010) Styles of interaction between aeolian, fluvial and shallow marine environments in the Pennsylvanian to Permian lower Cutler beds, south-east Utah, USA. *Sedimentology*, **57**, 1357–1385.

**Jungerius, P.D.** and **Dekker, L.** (1990) Water erosion in the dunes. In: *Dunes of the European Coast, Geomorphology, Hydrology, Soils* (Eds W.M. Bakker, P.D. Jungerius and J.A. Klijn), *Catena*, **18**, 185–193.

**Jungerius, P.D.** and **van der Meulen, F.** (1988) Erosion processes in a dune landscape along the Dutch coast. *Catena*, **15**, 217–228.

**Keefer, D.K.**, **Moseley, M.E.** and **deFrance, S.D.** (2003) A 38000-year record of floods and debris flows in the Ilo region of southern Peru and its relation to El Niño events and great earthquakes. *Paleogeogr. Paleocl. Paleoecol.*, **194**, 41–77.

**Kindler, P.**, **Davaud, E.** and **Strasser, A.** (1997) Tyrrhenian coastal deposits from Sardinia (Italy): a petrographic record of high sea levels and shifting climate belts during the last interglacial (isotopic substage 5e). *Palaeogeogr. Palaeoclimatol. Palaeoecol.*, **133**, 1–25.

**Kuhlemann, J.**, **Rohling, E.J.**, **Krumrei, I.**, **Kubik, P.**, **Ivy-Ochs, S.** and **Kucera, M.** (2008) Regional synthesis of mediterranean atmospheric circulation during the last glacial maximum. *Science*, **321**, 1338–1340.

**Lang, A.**, **Lindauer, S.**, **Kuhn, R.** and **Wagner, G.A.** (1996) Procedures used for optically and infrared stimulated luminescence dating of sediments in Heidelberg. *Ancient TL*, **14**, 7–11.

**Langford, R.P.** (1989) Fluvial-aeolian interactions: Part I, modern systems. *Sedimentology*, **36**, 1023–1035.

**Langford, R.P.** and **Chan, M.A.** (1989) Fluvial-aeolian interactions: Part II, ancient systems. *Sedimentology*, **36**, 1037–1051.

**Le Guern, P.** and **Davaud, E.** (2005) Recognition of ancient carbonate wind deposits: lessons from a modern analogue, Chrissi Island, Crete. *Sedimentology*, **52**, 915–926.

**Livingstone, I.** and **Warren, A.** (1996) *Aeolian geomorphology: An Introduction*. Longman Harlow, Essex, 211 pp.

**Loope, D.B.**, **Dingus, L.**, **Swisher, C.C.** and **Minjin, C.** (1998) Life and death in a Late Cretaceous dune field, Nemegt Basin, Mongolia. *Geology*, **26**, 27–30.

**Loope, D.B.**, **Mason, J.A.** and **Dingus, L.** (1999) Lethal sandslides from eolian dunes. *J. Geol.*, **107**, 707–713.

**Madsen, A.T.** and **Murray, A.S.** (2009) Optically stimulated luminescence dating of young sediments: a review. *Geomorphology*, **109**, 3–16.

**Martins, A.A.**, **Cunha, P.P.**, **Buylaert, J.P.**, **Huot, S.**, **Murray, A.S.**, **Dinis, P.** and **Stokes, M.** (2010) K-rich feldspar IRSL dating of a Pleistocene river terrace staircase sequence of the Lower Tejo River (Portugal, western Iberia). *Quatern. Geochron.*, **5**, 176–180.

**Martrat, B.**, **Grimalt, J.O.**, **Lopez-Martinez, C.**, **Cacho, I.**, **Sierro, F.J.**, **Abel Flores, J.**, **Zahn, R.**, **Canals, M.**, **Curtis, J.H.** and **Hodell, D.A.** (2004) Abrupt temperature changes in the Western Mediterranean over the past 250,000 years. *Science*, **306**, 1762–1765.

**Massari, F.** and **Parea, G.C.** (1988) Progradational gravel beach sequences in a moderate- to high-energy, microtidal marine environment. *Sedimentology*, **35**, 881–913.

**Mattheus, C.R.** and **Rodriguez, A.B.** (2011) Controls on late Quaternary incised-valley dimension along passive margins evaluated using empirical data. *Sedimentology*, **58**, 1113–1137.

**Mauz, B.**, **Bode, T.**, **Mainz, E.**, **Blanchard, H.**, **Hilger, W.**, **Dikau, R.** and **Zöller, L.** (2002) The luminescence dating laboratory at the University of Bonn: equipment and procedures. *Ancient TL*, **20**, 53–61.

**Mejdahl, V.** and **Christiansen, H.H.** (1994) Procedures used for luminescence dating of sediments. *Quatern. Sci. Rev.*, **13**, 403–406.

**Mirabella, A.**, **Costantini, E.A.C.** and **Carnicelli, S.** (1992) Genesis of a polycyclic Terra Rossa (Chromic Cambisol over Rhodic Nitosol) at the Poggio del Comune in Central Italy. *Z. Pflanzenbau. Bodenkunde*, **155**, 407–413.

**Moreno, A.**, **González-Sampériz, P.**, **Morellón, M.**, **Valero-Garcés, B.L.** and **Fletcher, W.J.** (2012) Northern Iberian abrupt climate change dynamics during the last glacial cycle: a view from lacustrine sediments. *Quatern. Sci. Rev.*, **36**, 139–153.

**Morton, D.M.**, **Alvarez, R.M.**, **Ruppert, K.R.** and **Goforth, B.** (2008) Contrasting rainfall generated debris flows from adjacent watersheds at Forest Falls, southern California, USA. *Geomorphology*, **96**, 322–338.

**Muhs, D.R.**, **Budahn, J.R.**, **Avila, A.**, **Skipp, G.**, **Freeman, J.** and **DeAnna, P.** (2010) The role of African dust in the formation of Quaternary soils on Mallorca, Spain and implications for the genesis of Red Mediterranean soils. *Quatern. Sci. Rev.*, **29**, 2518–2543.

**Murray, A.S.** and **Wintle, A.G.** (2000) Luminescence dating of quartz using an improved single-aliquot regenerative-dose protocol. *Radiat. Meas.*, **32**, 57–73.

**Muto, T.** and **Steel, R.J.** (2000) The accommodation concept in sequence stratigraphy: some dimensional problems and possible redefinition. *Sed. Geol.*, **130**, 1–10.

**Nanson, G.C.** and **Gibling, M.R.** (2003) Rivers and alluvial fans. In: *Encyclopedia of Sediments and Sedimentary*

*Rocks* (Ed G.V. Middleton), pp. 568–583, Encyclopedia of Earth Science Series, Kluwer Academic Press, London.

**Nemec, W.** and **Kanzaci, N.** (1999) Quaternary colluvium In the west-central Anatolia: sedimentary facies and palaeoclimatic significance. *Sedimentology*, **46**, 139–170.

**Nemec, W.** and **Postma, G.** (1993) Quaternary alluvial fans in southern Crete: sedimentation processes and geomorphic evolution. In: *Alluvial Sedimentation* (Eds M. Marzo and C. Puigdefabregas), *Int Assoc. Sedim. Special Publ.*, **17**, 235–276.

**Nichols, G.** and **Thompson, B.** (2005) Bedrock lithology control on contemporaneous alluvial fan facies, Oligo-Miocene, southern Pyrenees, Spain. *Sedimentology*, **52**, 571–585.

**Nielsen, K.A.**, **Clemmensen, L.B.** and **Fornós, J.J.** (2004) Middle Pleistocene magnetostratigraphy and susceptibility sratigraphy. Data from carbonate aeolian system, Mallorca, Western Mediteranean. *Quatern. Sci. Rev.*, **23**, 1733–1756.

**Nott, J.**, **Thomas, M.F.** and **Price, D.M.** (2001) Alluvial fans, landslides and Late Quaternary climatic change in the wet tropics of northeast Queensland. *Aust. J. Earth Sci.*, **48**, 875–882.

**Nott, J.**, **Haig, J.**, **Neil, H.** and **Gillieson, D.** (2007) Greater frequency variability of landfalling tropical cyclones at centennial compared to seasonal and decadal scales. *Earth Planet. Sci. Lett.*, **255**, 367–372.

**Ortiz, I.**, **Simón, M.**, **Dorronsoro, C.**, **Martín, F.** and **García, I.** (2002) Soil evolution over the Quaternary period in a Mediterranean climate (SE Spain). *Catena*, **48**, 131–148.

**Pérez Alberti, A.**, **Valcárcel Díaz, M.**, **Martini, I.P.**, **Pascucci, V.** and **Andreucci, S.** (2011) Upper Pleistocene, mid-latitude, mountain glacial landscape and sediments at Pias, NW Spain. In: *Ice-Marginal and Periglacial Processes and Sediments* (Eds I.P. Martini, H.M. French and A. Pérez Alberti). *Geol. Soc. London Spec. Pub.*, **355**, 93–110. doi: 10.1144/SP354.6

**Posamentier, H.W.** and **Vail, P.R.** (1988) Eustatic control on clastic deposition: II. Sequence and systems tracts models. In: *Sea Level Changes: An Integrated Approach* (Eds C.K. Wilgus, B.S. Hastings, C.G.St.C. Kendall, H.W. Posamentier, C.A. Ross and J.C. Van Wagoner), *SEPM Spec. Publ.*, **42**, 125–154.

**Prescott, J.R.** and **Hutton, J.T.** (1994) Cosmic ray contribution to dose rates for luminescence and ESR dating: large depths and long-term time variations. *Radiat. Meas.*, **23**, 497–500.

**Rahmstorf, S.** (2002) Ocean circulation and climate during the past 120,000 years. *Nature*, **419**, 207–214.

**Reimer, P.J.**, **Baillie, M.G.L.**, **Bard, E.**, **Bayliss, A.**, **Beck, J.W.**, **Blackwell, P.G.**, **Bronk Ramsey, C.**, **Buck, C.E.**, **Burr, G.S.**, **Edwards, R.L.**, **Friedrich, M.**, **Grootes, P.M.**, **Guilderson, T.P.**, **Hajdas, I.**, **Heaton, T.J.**, **Hogg, A.G.**, **Hughen, K.A.**, **Kaiser, K.F.**, **Kromer, B.**, **McCormac, F.G.**, **Manning, S.W.**, **Reimer, R.W.**, **Richards, D.A.**, **Southon, J.R.**, **Talamo, S.**, **Turney, C.S.M**, **van der Plicht, J.** and **Weyhenmeyer, C.E.** (2009) IntCal09 and Marine09 radiocarbon age calibration curves, 0-50,000 years cal BP. *Radiocarbon*, **51**, 1111–1150.

**Ritter, J.B.**, **Miller, J.R.** and **Husek-Wulforst, J.** (2000) Environmental controls on the evolution of alluvial fans in Buena Vista valley, North central Nevada, during Late Quaternary time. *Geomorphology*, **36**, 63–87.

**Roberts, H.M.** and **Wintle, A.G.** (2001) Equivalent dose determinations for polymineralic fine-grains using the SAR protocol: application to a Holocene sequence of the Chinese Loess Plateau. *Quatern. Sci. Rev.*, **20**, 859–863.

**Rodríguez-López, J.P.**, **Meléndez, N.**, **De Boer, P.** and **Soria, A.R.** (2010) The action of wind and water in a mid-Cretaceous subtropical erg-margin system close to the Variscan Iberian Massif, Spain. *Sedimentology*, **57**, 1315–1356.

**Scherer, C.M.S.**, **Lavina, E.L.C.**, **Filho, D.C.D.**, **Oliveira, F.M.**, **Bongiolo, D.E.** and **Aguiar, E.S.** (2007) Stratigraphy and facies architecture of the fluvial–aeolian–lacustrine Sergi Formation (Upper Jurassic), Recôncavo Basin. Brazil. *Sed. Geol.*, **194**, 169–193.

**Shanley, K.W.** and **McCabe, P.J.** (1994) Perspectives on the sequence stratigraphy of continental strata. *Am. Assoc. Petrol. Geol Bull.*, **78**, 544–568.

**Siddal, M.**, **Chappell, J.** and **Potter, E.K.** (2007) Eustatic Sea level during past interglacials. In: *The Climate of Past Interglacials* (Eds. F. Sirocko, M. Claussen, M.F. Sanchez-Goñi and T. Litt), *Dev. Quatern. Sci.*, **7**, 75–92.

**Sloss, C.R.**, **Jones, B.G.**, **Switzer, A.D.**, **Nichol, S.**, **Clement, A.J.H.** and **Nicholas, A.W.** (2009) The Holocene infill of Lake Conjola, a narrow incised valley system on the southeast coast of Australia. *Quatern. Int.*, **221**, 23–35.

**Smith, B.W.**, **Rhodes, E.J.**, **Stokes, S.**, **Spooner, N.A.** and **Aitken, M.J.** (1990) Optical dating of sediments: initial quartz results from Oxford. *Archaeometry*, **32**, 19–31.

**Sohn, M.F.**, **Mahan, S.A.**, **Knott, J.R.** and **Bowman, D.D.** (2007) Luminescence ages for alluvial-fan deposits in Southern Death Valley: Implications for climate-driven sedimentation along a tectonically active mountain front. *Quatern. Int.*, **166**, 49–60.

**Spencer, J.Q.G.** and **Robinson, R.A.J.** (2008) Dating intramontane alluvial deposits from NW Argentina using luminescence techniques: problems and potential. *Geomorphology*, **93**, 144–155.

**Stokes, S.** (1992) Optical dating of young (modern) sediments using quartz: results from a selection of 26 depositional environments. *Quatern. Sci. Rev.*, **11**, 153–159.

**Svendsen, J.**, **Stollhofen, H.**, **Krapf, C.B.E.** and **Stanistreet, I.G.** (2003) Mass and hyperconcentrated flow deposits record dune damming and catastrophic breakthrough of ephemeral rivers, Skelton Coast Erg, Namibia. *Sed. Geol.*, **160**, 7–31.

**Sweeney, M.R.** and **Loope, D.B.** (2001) Holocene dune-sourced alluvial fans in the Nebraska Sand Hills. *Geomorphology*, **38**, 31–46.

**Talbot, M.R.** and **Williams, M.A.J.** (1978) Erosion of fixed dunes in the Sahel, central Niger. *Earth Surf. Proc.*, **3**, 107–113.

**Talbot, M.R.** and **Williams, M.A.J.** (1979) Cyclic alluvial fan sedimentation on the flanks of fixed dunes, Janjari, central Niger. *Catena*, **6**, 43–62.

**Thiel, C.**, **Buylaert, J.-P.**, **Murray, A.S.**, **Terhorst, B.**, **Hofer, I.**, **Tsukamoto, S.** and **Frechen, M.** (2011) Luminescence dating of the Stratzing loess profile (Austria) – testing the potential of an elevated temperature post-IR IRSL protocol. *Quatern. Int.*, **234**, 23–31.

**Thompson, C.H.** (1983) Development and weathering of large parabolic dune systems along the subtropical coast of eastern Australia. *Ann. Geomorphol.*, **45**, 205–225.

**Viseras, C.**, **Calvache, M.L.**, **Soria, J.M.** and **Fernández, J.** (2003) Differential features of alluvial fans controlled by tectonic or eustatic accommodation space. Examples from the Betic Cordillera, Spain. *Geomorphology*, **50**, 181–202.

**Waelbroeck, C.**, **Labeyrie, L.**, **Michel, E.**, **Duplessy, J.C.**, **McManus, J.F.**, **Lambeck, K.**, **Balbon, E.** and **Labracherie, M.** (2002) Sea-level and deep water temperature changes derived from benthic foraminifera isotopic records. *Quatern. Sci. Rev.*, **21**, 295–305.

**Wintle, A.G.** and **Murray, A.S.** (2006) A review of quartz optically stimulated luminescence characteristics and their relevance in single-aliquot regeneration dating protocols. *Radiat. Meas.*, **41**, 369–391.

*Manuscript received 16 April 2012; revision accepted 23 May 2013*